

THE QUANTITATIVE ANALYSIS OF CORONAL SUTURE SEPARATION DUE TO
CRANIAL TRAUMA

A Thesis

Presented to

The Faculty of the Department of Biological Sciences
Sam Houston State University

In Partial Fulfillment

of the Requirements for the Degree of

Master of Science

by

Stephanie Anne Baker

May, 2022

THE QUANTITATIVE ANALYSIS OF CORONAL SUTURE SEPARATION DUE TO
CRANIAL TRAUMA

by

Stephanie Anne Baker

APPROVED:

Patrick J. Lewis, PhD
Committee Director

Monte L. Thies, PhD
Committee Member

Aaron M. Lynne, PhD
Committee Member

John Pascarella, PhD
Dean, College of Science Engineering
and Technology

DEDICATION

I dedicate this thesis to my parents, Shirley and Steven Baker.

ABSTRACT

Baker, Stephanie Anne, *The quantitative analysis of coronal suture separation due to cranial trauma*. Master of Science (Biology), May, 2022, Sam Houston State University, Huntsville, Texas.

Morphometric analysis of cranial sutures can provide evidence of microfractures, diastasis, and early sutural closure. Recently, mCT has allowed for morphometric analyses on much smaller scales and has been used to differentiate normal cranial sutures from early sutural synostosis. Therefore, microscopic assessment of cranial sutures may provide additional data to forensic trauma analyses. Utilizing six adult human cranial trauma cases and three control specimens, I tested for asymmetrical separation in coronal sutures to determine if significant differences are detectable. Trauma cases included three intraoral gunshot wound and three blunt force trauma specimens. Cranial specimens were mCT scanned with Type-1 landmarks placed at their origin at sphenion and terminating at bregma. Due to the tortuous nature of the coronal suture, a comb-based approach was used to standardize sampling sites. Using Avizo segmenting software (Thermo Fisher Scientific), a chord line between bregma and sphenion was first defined and measured, which allowed for the placement of 20 and 50 equidistant sampling sites along the suture at orthogonal angles. ImageJ was used to calculate the total area of separation for individual scan slices at each sampling site. Asymmetry was determined by comparing differences in coronal suture separation between the sides delineated by bregma. Additionally, Avizo was used to segment total sutural volume using in program measuring tools. Bilateral asymmetry of coronal diastasis per specimen was determined using a paired t-tests. A one-way ANOVA was then used to test total coronal sutural separation by group. One-way ANOVAs were also used to test average control group

diastasis with diastasis on the side of trauma groups both with and without damage. Finally, a two-way repeated measures ANOVA was used to determine if significant differences occur both within and between traumatized specimens. Results from paired t-tests showed significant differences between sides in individual crania using different numbers of landmarks. Alternately, no significant differences were found for overall coronal diastasis, side specific separation, or within trauma type using repeated measures. Ultimately, these data could potentially provide forensics with another method to assess injury and may lead to a more thorough understanding of sutural diastasis in human crania.

KEY WORDS: Cranial suture, Coronal suture, Micro-computed tomography, Avizo, Forensic anthropology, Cranial trauma, Ballistic trauma, Blunt force trauma

ACKNOWLEDGEMENTS

First, I would like to thank you my parents, Shirley and Steven Baker, and my sister, Suzanne Knobel, and brother in law, Morgan Knobel for all of their support and encouragement. It has been a long road, but I could not have done it without you. A special thank you to my mother who has been my biggest champion and inspiration.

I want to also thank my thesis committee members Drs. Patrick Lewis, Monte Thies, and Aaron Lynne for all of their edits and encouragement throughout my master's degree. I have taken classes from all three professors in my undergraduate and master's degrees and they have been instrumental in shaping the scientist that I am today. I owe an immeasurable amount of gratitude to Dr. Patrick Lewis, who has provided guidance and moral support not only during my master's degree, but also in every endeavor during my time here at SHSU. A huge thank you to the family of Mr. Joey Harrison whose scholarship I was fortunate enough to receive to fund part of this study – I cannot thank you enough. Also, I would like to thank Dr. Tim Campbell and Dr. Juan Daza for helping me formulate my mCT sampling strategies, statistics help, and constant support though the many hours spent in front of the computer segmenting.

Thank you to Dr. Joan Bytheway, Dr. Sheree Hughes and Hailey Kennedy at the STAFS facility and Dr. Danny Wescott and Dr. Deborah Cunningham from the FACTS facility for allowing me to analyze the specimens. Similarly, thank you to Dr. Jessie Maisano, Dr. Matt Colbert, and Dave Edey at UTCT for scanning the specimens.

Last, but certainly not least, I would like to thank the families and individuals who have donated themselves or loved ones to the STAFS and FACTS facilities. Without their generous donation, this thesis would not have been possible.

TABLE OF CONTENTS

	Page
DEDICATION	iii
ABSTRACT	iv
ACKNOWLEDGEMENTS	vi
TABLE OF CONTENTS.....	vii
LIST OF TABLES	ix
LIST OF FIGURES	xi
CHAPTER I: INTRODUCTION	1
Macroscopic Anatomy of Sutures	2
Microscopic Anatomy of Sutures	6
Embryology of Suture Formation.....	7
Cranial Suture Closure.....	8
CHAPTER II: MECHANICAL PROPERTIES OF BONE	12
Introduction to Mechanics	12
Biomechanics of Bone Tissue	15
Mechanical Properties of Cortical Bone.....	16
The Mechanical Effects of Loading on Bone	17
CHAPTER III: TRAUMA TYPES, TIMING OF INJURIES, AND FRACTURES	19
Timing of Injuries	19
Blunt Force Trauma.....	21
Ballistic Trauma.....	25
Research Hypothesis / Objectives	28
H ₀ : Hypothesis	28

CHAPTER IV: MATERIALS AND METHODS.....	29
CHAPTER V: RESULTS	48
CHAPTER VI: DISCUSSION AND CONCLUSION.....	59
REFERENCES	64
VITA.....	76

LIST OF TABLES

Table	Page
1 Age of Specimens, Manner of Death, and Side of Trauma for Cranial Examined in this Study	39
2 Left And Right Chord Lengths from Bregma to Sphenion and Distance Between Landmarks for Each of the Crania Scanned	41
3 Summed Total Area of Complete Coronal Suture Separation using 10, 20, 25, and 50 Landmarks.....	44
4 Total Area of Left and Right Coronal Suture Separation Per Specimen.....	45
5 Total Left and Right Sutural Areas with 10 Landmarks.....	48
6 Total Left and Right Sutural Areas with 20 Landmarks.....	49
7 Total Left and Right Sutural Areas with 25 Landmarks.....	50
8 Total Left and Right Sutural Areas with 50 Landmarks.....	51
9 One-Way Anova Comparing Total Sum of Sutural Separation among Groups..	53
10 One-Way Anova with Total Average Sum of Control Specimens and Total Area of Side with Trauma	54
11 One-Way Anova with Total Average Sum of Control Specimens and Total Area of Contralateral Side of Trauma	55
12 Two-Way Repeated Measures Anova Comparing Trauma Types and Side	56
13 One-Way Anova Results Comparing Total Volume among Specimens.....	57
14 One-Way Anova with Average Sum of Control Specimen Volume and Side of Trauma.....	57

15 One-Way Anova with Average Sum of Control Specimen Volume and Side of No Trauma.....	57
16 Two-Way Repeated Measures Anova Comparing Trauma Type and Side Volumes.....	58

LIST OF FIGURES

Figure		Page
1	Cranial Suture Anatomy of The Adult Skull	4
2	Examples of a serrated sagittal suture interlocking the left and right parietal bones	6
3	Stress-Strain Curve (Young's Modulus)	14
4	Bone's Load-Displacement Curve. See the Text above for an Explanation of the Curve.....	17
5	Buttresses of the Cranial Vault	23
6	Buttresses of the Face	24
7	Le Fort Fracture Types of the Face. See the Text for a Description of each Fracture Type.....	24
8	Depictions of Radiating and Concentric Fractures on the Cranium Resulting from a Gunshot Wound	26
9	Control Specimen, STAFS 2011-005	30
10	Control Specimen, FACTS 2013-016.....	31
11	Control Specimen, FACTS 2015-007.....	32
12	Blunt Force Trauma Specimen, STAFS 2014-012.....	33
13	Blunt Force Trauma Specimen, FACTS 2011-022	34
14	Blunt Force Trauma Specimen, FACTS 2013-057	35
15	Intra-Oral Gunshot Wound Specimen, STAFS 2017-017.....	36
16	Intra-Oral Gunshot Wound Specimen, FACTS 2013-046	37
17	Intra-Oral Gunshot Wound Specimen, FACTS 2013-019	38

18	Imaging of the Right and Left Sides of the Coronal Suture	40
19	Comb-Based Sampling Approach to Standardize Sampling Sites	42
20	Total Sutural Area at Sampling Site	43
21	View of Segmented Suture	46

CHAPTER I

Introduction

Following traumatic or suspicious deaths, it is the job of pathologists and forensic anthropologists to evaluate macroscopic and microscopic changes to both soft and hard tissues (Blau, 2016). However, when remains are in advanced decomposition or skeletonized, pathologists can no longer rely on soft tissue damage to identify trauma but must look to the expertise of forensic anthropologists (Fenton et al., 2005; Moraitis et al., 2008). A forensic anthropologist uses skeletal trauma to reconstruct peri- and post-mortem events that caused injury or death of an individual (Hart, 2005; Kranioti, 2015; Poikines and Symes, 2013; Sorg et al., 2017).

In addition to the biological profile (e.g., ancestry, sex, age, stature), bones provide information regarding the type of trauma inflicted (Poikines and Symes, 2014; Sorg et al., 2017). Skeletal trauma is an alteration and ultimate failure of bone at the macro- and/or microscopic level in cortical and/or trabecular bone caused by a slow and/or rapid load impact with an object (Blau, 2016). The cranial region is commonly affected by trauma and is one of the most complicated to understand (Mortiz, 1954). In particular, when trauma to the skull occurs, fracture lines follow areas of weakness and terminate at areas of interruption in the bones, such as another fracture line or a cranial suture (Byers, 2017; Fenton et al., 2005). Current methods rely predominantly on macroscopic observation of the trauma. While macroscopic examination can reveal valuable information, it can also be inconclusive or misrepresentative. However, with the development of imaging techniques such as microcomputed tomography (mCT) technology, trauma that may not be observed macroscopically can be assessed.

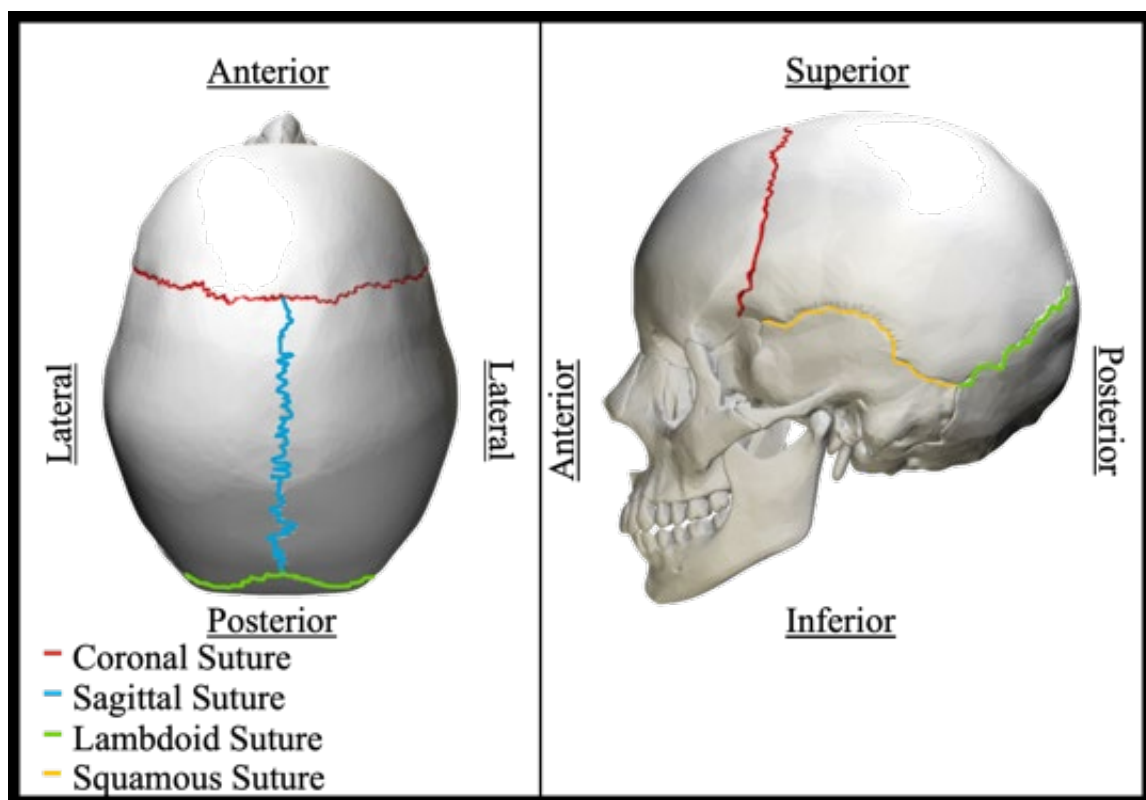
Cranial sutures are synarthrodial joints that form fibrous articulations between the margins of adjacent bones in the vertebrate crania while providing mechanical support and flexibility (Chopra, 1957; Liu et al., 2017; Maloul et al., 2013). Twenty-three sutures are recognized in the average adult human skull: 10 are located in the calvarium, and the other 13 articulate bones of the face (Baker, 1984). The first documented descriptions of cranial sutures are from the Edwin Smith Surgical Papyrus of ancient Egyptians, written around 1600 B.C. (Serageldin, 2013). Since then, much of the forensic literature has focused on using cranial sutures to estimate age at death. However, little research has been done to examine how trauma affects the sutures of the skull. Therefore, understanding how trauma affects the crania on a microscopic level through the use of mCT scans may provide additional information about the individual's death.

Macroscopic Anatomy of Sutures

The bones of the cranial vault have a unique diploic construction, where trabecular bone is sandwiched between two layers of cortical bone and function to protect the brain from trauma while also reducing the weight of the skull (Wood, 1971; Goldsmith, 1972; Meschan, 1974; Akkas, 1975). The outer table forms the ectocranial surface while the inner layer forms the endocranial surface. The endocranial layer is usually thinner than the outer table (Miroué, 1975).

The main sutures of the skull are the coronal, sagittal, lambdoid and squamosal sutures (Figure 1). The coronal suture is located on the anterior aspect of the skull at the junction of the frontal and parietal bones (White et al., 2012). The sagittal suture is located between the two parietal bones and extends from bregma (intersection of the coronal and sagittal sutures) to lambda (intersection of the sagittal and lambdoid sutures)

(White et al., 2012). The squamosal suture separates the parietal from the temporal bone on the lateral aspects of the cranium. The lambdoid suture is located posteriorly on the cranium and connects the two parietal bones to the occipital bone. Another prominent suture found on the anterior aspect of the skull is the metopic or frontal suture (*sutura interfrontalis*). The metopic suture is present in individuals less than two years of age but generally fuses completely and obliterates. However, this suture remains patent in some individuals until adulthood and throughout life and can be used in ancestry determination (Krogman and Iscan, 1986). Similarly, other cranial vault sutures include the sphenofrontal, sphenotemporal, sphenoparietal, and occipitomastoid sutures. Non-cranial vault sutures that connect the facial region to the base of the skull include the zygomaticomaxillary, frontonasal, and frontomaxillary sutures (White et al., 2012).

Figure 1*Cranial Suture Anatomy of The Adult Skull*

Classification of sutures is generally based on their articulation between the edges of bone; however, sutures can also be classified based on their degree or complexity (Herring, 1972). In classification by articulation, sutures are described as simple or overlapping based on the orientation of the bone surfaces (Saladin, 2018). Therefore, simple sutures have both bone surfaces in the same or similar plane while overlapping sutures have two surfaces articulating in different planes. Simple sutures, or end-to-end, butt, flat, or plane sutures, are typically found in the sagittal plane (Cohen, 1993; De Coster et al., 2007; Saladin, 2018). An example of a simple suture is the palatine suture (Mann et al., 1991; Gruspier and Mullen, 1991; Ginter, 2005). An overlapping or beveled

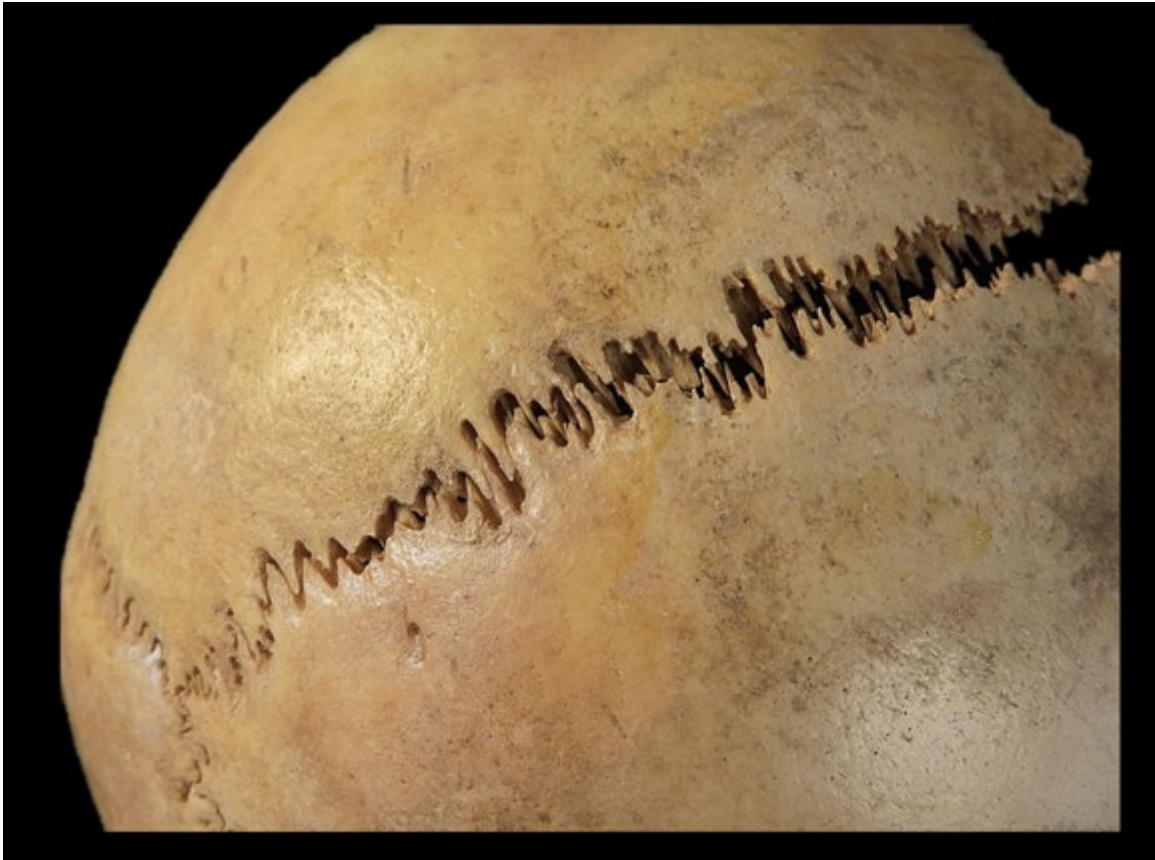
suture can be analogously compared to overlapping tiles on a roof, thereby increasing the articulating surface area and offering greater resistance at the sutural edge (Herring, 1972). The squamous suture, found between the parietal and temporal bones, is an example of an overlapping suture.

Sutures are also classified based on the number of interdigitations found in the suture pattern (Herring, 1972). Specifically, a simple suture has fewer interdigitations than a serrated suture which have greater interdigitations and a jagged appearance. Serrated sutures appear as wavy lines that interlock the adjoining bones of the cranium by their serrated margins (Figure 2). Examples include the coronal, sagittal and lambdoid sutures. However, a single suture may be classified differently along its length as they traverse large areas on the skull (Krogman and Iscan, 1986). Initially, it was believed that all sutures originate as a simple suture in development and then become interdigitated (Wagemans et al., 1988; Cohen, 1993). Wu and colleagues (2007) demonstrated that the sagittal suture increases in irregularly and complexity with age; however, this complexity only occurs until the age of 10 years.

Ectocranial and endocranial sutures also differ in their patterns and complexities. Ectocranial sutures have generally diverse suture patterns with simple and complex interdigitations. Endocranial sutures, found on the inner aspect of the skull, are simple and homogenous in their arrangements (Hauser and De Stefano, 1989).

Figure 2

Examples of a Serrated Sagittal Suture Interlocking the Left and Right Parietal Bones

**Microscopic Anatomy of Sutures**

Cranial sutures undergo the most growth during early development, from simple flat joints to interdigitating and interlocking projections in adulthood (Maloul et al., 2010; Maloul et al., 2013; Liu et al., 2017). Cranial sutures are composed of stiffer skeletal components than the cranial bones and connect via soft tissue (Liu et al., 2017).

Specifically, bones forming the sutures are linked through fibrous mesenchymal tissue referred to as the sutural ligament. Pritchard et al. (1956) defined five layers of the sutural ligament. The cambial layers are located on both sides of the bone's sutural aspect and

contain osteogenic cells. Fibrous capsular layers are located on the medial aspects of the cambial layers. Lastly, the middle layer is highly vascular and contains the blood vessels and nerves that supply the joint. The blood vessels in the middle layer of the suture also link the diploic veins, intracranial venous sinuses, and external veins of the scalp (Pritchard et al., 1956; Cohen, 1993; Proff et al., 2006); however, the cambial and fibrous capsular layers are continuous with the periosteum both internally and externally along the sutural margins (Prichard et al., 1956; Moss, 1960).

Embryology of Suture Formation

In fetal development, the vault of the skull forms part of the membranous neurocranium and is derived from the primitive meninx of the mesoderm found around the developing neural tube. Specifically, the primitive meninx is divided into the ectomeninx (located externally) and the endomeninx (located internally) (Harrison, 1978). The endomeninx gives rise to the pia and arachnoid mater, and the ectomeninx will form the bones of the cranial vault and dura mater of the brain. The ectomeninx forms a membrane that undergoes intramembranous ossification to form the frontal, parietal, parts of the occipital, and the squamous portion of the temporal bone.

At the eighth embryonic week, ossification centers of the skull start to appear. The ossification centers allow bone to grow from the center towards the margin of the adjacent bone (Harrison, 1978; Hauser and De Stefano, 1989). Initially, the bones are connected by a dense layer of connective tissue, which ultimately gives rise to the sutures. However, the edges of the cranial vault bones do not fuse but overlap each other to allow the large skull of the fetus to pass through the birth canal (Cohen, 1993).

At birth, certain regions of the skull have fontanelles, which are large areas that separate the bones from one another where ossification is not complete (Dryden, 1978; Langman, 1981). The anterior fontanelle is located between the frontal and parietal bones and is the last fontanelle to close around two years of age, while the other fontanelles close at the end of the first year (Kirmi et al., 2009). These fontanelles close at different times, allowing the cranial vault to expand and grow during the first year of life (Kirmi et al., 2009). Cranial vault bone growth is directed by the growth of the brain and other factors such as tissue interactions at sutural sites, signaling of the dura mater by specific cells, and physical forces produced by the expansion of the skull (Ogle et al., 2004). As the bones of the cranial vault grow, the fontanelles will decrease in size and form into the sites for the sutures of the skull.

At birth, the bones of the skull are unilamellar and have not yet differentiated into the two layers of compact bone separated by cancellous bone. Suture formation occurs during the first and second years of extra-uterine life and do not change significantly in appearance until adulthood. The bones of the skull interlock at the sutures by tongue-shaped processes called “lingulae,” with the internal and external lingulae developing differently (Oudhof, 1982; Hauser and De Stefano, 1989).

Cranial Suture Closure

The process of cranial suture closure is contingent upon numerous interactions and varies considerably across adults (Furuya et al., 2009). With the exception of the metopic suture, sutures generally fuse from back-to-front and laterally-to-medially (Kirmi et al., 2009). There are varying reports of age and sutural closure reported in the literature. Dwight (1890) reported open or patent cranial vault sutures at 80 years of age,

while the same sutures in other individuals may be completely obliterated before 50 years of age. Kirmi and colleagues (2009) noted that the coronal, lambdoid, and sagittal sutures will remain patent until the fourth decade of life whereas Furuya (1984) reported that sutures could be identified into the seventh decade. Despite the erratic patterns of ectocranial suture fusion, endocranial sutures close earlier than ectocranial sutures (Christensen et al., 2014).

In some New World monkeys, the circum-mental (parieto-squamosal, parieto-mastoid, occipito-mastoid, spheno-temporal, spheno-frontal, and spheno-parietal) sutures remain patent throughout life (Chopra, 1957). However, cranial sutures in peccaries (*Tayassuidae*) fuse early due to the animals using their snout to root for food at a very early age (Herring, 1974).

In biological anthropology, cranial sutures have been used to determine age at time of death despite the erratic patterns of suture fusion (Todd and Lyon, 1924; Todd and Lyon, 1925a; Todd and Lyon, 1925b; Todd and Lyon, 1925c; Acsadi and Nemeskeri, 1970; Meindl and Lovejoy, 1985; Krogman and Iscan, 1986) and ancestry determination by specific sutural patterns among individuals (Sekharan, 1985; Rogers and Allard, 2004). Specifically, the sutures most commonly used for age estimation are located in the vault of the skull. The three most prominent vault sutures are the coronal, sagittal, and lambdoid suture.

Sutures were once considered to close and obliterate when the growth and development of the skull ceased (Kokich, 1986). However, the study of the fusion of the cranial sutures has been dominated by the investigation of craniosynostosis or the premature fusion of one or more sutures of the skull, usually occurring in the first year of

life (Bolk, 1917; Cohen, 1993; Kimonis et al., 2007; Slater et al., 2008; Kirmi et al., 2009; Iyengar et al., 2015). The most common suture to exhibit craniosynostosis is the sagittal suture, followed by the unilateral coronal and/or bilateral coronal, metopic, and lambdoid sutures.

Facial sutures demonstrate greater connectivity than those of the cranial vault, which will undergo considerable yield and plastic deformation before failure (Maloul et al., 2010). Craniofacial sutures often fail at the separation through the suture or exhibit a fracture extending away from the sutural site, indicating that the sutures were weaker than the adjacent cranial bones (Maloul et al., 2013). However, in trauma cases involving children, diastasis of cranial sutures is common due to the lack of cranial bone ossification, unfused sutures, and exposed fontanelles (Campobasso et al., 2019). The malleability of juvenile skulls allows for increased resistance to fracture (Byers, 2017; Campobasso et al., 2019). Campobasso et al. (2019) presented a case of an undetected traumatic diastasis of the coronal and sagittal sutures of a 7-year-old boy, noting that cranial diastasis can be wrongly interpreted due to the unfused bones of the juvenile skull. Consequently, traumatic head injuries can be easily misinterpreted due to unique features related to the age of the individual and the type of imaging used (Campobasso et al., 2019).

Macroscopic assessment of cranial suture ossification has been widely viewed as unreliable and highly variable, shifting current examinations to alternate imaging techniques such as mCT technology (Furuya et al., 1984; Sherick et al., 2000; Harth et al., 2009; Corega et al., 2010). Imaging technologies such as SEM and mCT scans have increased the ability of forensic investigators to analyze trauma nondestructively (Becker,

2002; Li et al., 2013). While these images are typically created in 3D, any 2D slice of the scan can be extracted, viewed, and analyzed (Li et al., 2013). Computed tomography scans are often used to evaluate areas of complex trauma (Myers, 1999), are non-destructive and can provide an additional method to assess trauma (Myers, 1999; Li et al., 2013).

Considerable research has been dedicated to the analysis of cranial suture closure or synostosis. For example, Harth et al. (2009) examined the internal structural segments of the sagittal, coronal, and lambdoid sutures to determine if there was a correlation between age and stages of sutural closure using mCT technology. Sherick et al. (2000) examined and assessed the ability of a mCT scanner to view normal and synostosed cranial sutures. Similarly, Corega et al. (2010) evaluated normal and synostosed cranial suture morphology at the microscopic level using samples from the coronal suture of two children aged 1.3 and 1.5 years old.

While various studies have been conducted using mCT in the analysis of cranial suture synostosis (Furuya et al., 1984; Sherick et al., 2000; Harth et al., 2009; Corega et al., 2010), no peer reviewed mCT-based studies of suture area in traumatized adult human crania could be found. Due to the tortuous nature of the sutures of the human crania, this study presents a novel mCT comb-based approach to standardize sampling sites along the coronal suture. This analysis may be applicable to other complex sutures of the skull where sampling site standardization may be difficult. Furthermore, this study seeks to establish a protocol for standardization of sampling sites of the coronal suture using mCT segmenting software, Avizo (Thermo Scientific).

CHAPTER II

Mechanical Properties of Bone

In the skeleton, the geometry, composition, and relative thickness of bones dictate their mechanical properties, thereby determining the extent of potential deformation during trauma (Wedel and Galloway, 2014; Lillie, 2015). Before describing the mechanical properties of bone, the terminology of mechanics is briefly discussed.

Introduction to Mechanics

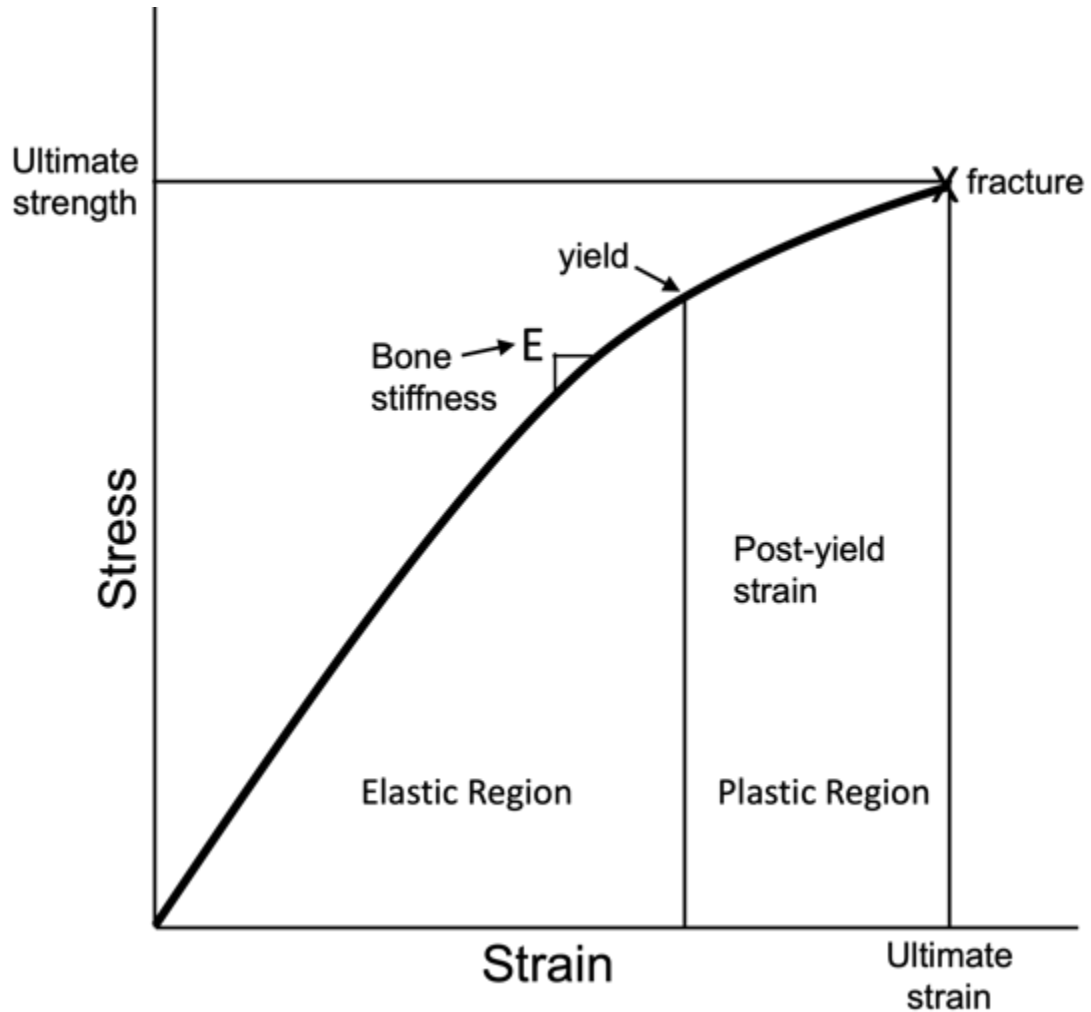
Mechanics, the science that studies the effects of forces upon the form or motion of bodies, can be divided into two groups, statics and dynamics (Rogers, 2010). Statics is the study of bodies at rest or in equilibrium as a result of forces acted upon them and dynamics is the study of moving bodies. Most materials are usually studied under static conditions that easily permit the observation of the applied forces or load.

A force is anything that changes the state of a body or object with respect to its motion or position (Rogers, 2010). There are three primary types of forces: compressive or pushing forces, tensile or pulling apart forces, and shearing or sliding forces that make one part of the body slide with respect to an adjacent part (Martin et al., 1998). If a force is applied to a body, it produces stresses and strains within the body (Martin et al., 1998). Stress is defined as a ratio between the force and the area upon in which the force is acting, indicated in terms of pounds of force or kilograms of force per unit area (Hart et al., 2017). Strain is defined as a change in the linear dimension of a body as a result of the application of the force (Rogers, 2010; Hart et al., 2017).

The maximum stress and strain a material can sustain are designated as the ultimate strength and ultimate strain. The relationship between the stress and strain is

denoted by a stress-strain curve (Martin et al., 1998). The slope of the stress-strain curve within the elastic region is called the modulus of elasticity, or Young's modulus (Martin et al., 1998; Byers, 2017). Young's modulus is a measure of the stiffness of a material, not its elasticity which is the property of a material that allows it to return to its original dimension upon removal of the force or load (Turner, 2006). The area under the stress-strain curve is a measure of the amount of energy needed to induce failure (Byers, 2017).

The elastic strain region of a material describes the deformation as being reversible and the plastic strain region of a material is irreversible deformation before failure (Turner, 2006; Hart et al., 2017). Young's modulus is separated by the yield point, which represents a gradual transition in which the stresses begin to cause irreversible permanent damage to the material (Figure 3). The yield point is also that point where the stress-strain curve becomes nonlinear. The post-yield strain is inversely proportional to the brittleness of bone (Turner, 2006; Currey, 2012). A material is determined to be brittle when it breaks without presenting any irreversible post-yield deformation (Turner 2006). Determining if a material is brittle does not provide any direct information about how much stress it can tolerate; however, the presence or absence of post-yield deformation is a crucial feature of the mechanical properties of a material. Materials that exhibit a reasonable amount of post-yield deformation are often tough (Turner, 2006). A tough material is one that is resistant to cracking and is usually able to absorb a great deal of energy before breaking (Currey, 2012).

Figure 3*Stress-Strain Curve (Young's Modulus)*

An isotropic material is described as having properties that are the same in all directions while anisotropic materials vary in different directions (Currey, 2012). Bone is described as being an anisotropic material and will vary under the different kinds of mechanical behavior according to the direction of the applied force or load (Martin et al., 1998; Currey, 2012; Hart et al., 2017).

Biomechanics of Bone Tissue

Bone tissue is a two-phase porous anisotropic material composed primarily of tough collagen packed with rigid calcium phosphate mineral. Mechanical properties of bone are largely determined by the amount, spatial arrangement, molecular structure, and quality of these components (Turner, 2006; Currey, 2012).

The stiffness of bone is primarily associated with mineral content; however, if too much mineralization occurs bone becomes brittle and requires less energy to fail and fracture (Turner, 2006). The collagen matrix associated with the toughness of bone making it less brittle and more resistant to fracturing (Turner, 2006). The ratio of mineral content to collagen affects bone's strength and brittleness (Hart et al., 2017). If bone has excessive mineral content or undergoes changes in mineral quality, brittleness increases. Excessive collagen, however, improves the overall bone toughness but has little influence on the strength and stiffness of bone (Hart et al., 2017).

The mechanical properties of bone are governed by the same principles as those described above. Strength and stiffness of a bone is a product of its shape, size, and strength of materials within that bone (Turner, 2006). Similarly, the mechanical properties of bone require the balance of many demands placed upon them. The skeleton provides a support system for muscles that work against each other in order to create motion and maintain posture. The stiffer the bone, the more efficient the action of the muscles are at producing movement. If the bone is less stiff, part of the mechanical output of the muscles is used in the bone deformation process rather than in creating motion (Martin et al., 1998).

Another consideration is the weight of bone, since the stronger the bone the more weight it can support and carry around (Currey, 2012). The overall mechanical properties of bone represent a compromise between the need for stiffness to make muscle action efficient and the need for compliance to absorb the energy placed upon them without fracturing, all while minimizing skeletal weight (Martin et al., 1998; Turner, 2006).

There are a number of biomechanical parameters that can be applied to describe the integrity of bone. The load-displacement curve is a relationship between the applied load and displacement response (Figure 4; Turner, 2006). The slope of the elastic region of the curve (S) denotes the extrinsic stiffness or rigidity of the overall bone structure. A number of other biomechanical properties can be derived from the curve, including ultimate force (F_u), work to failure (U), and ultimate displacement (d_u).

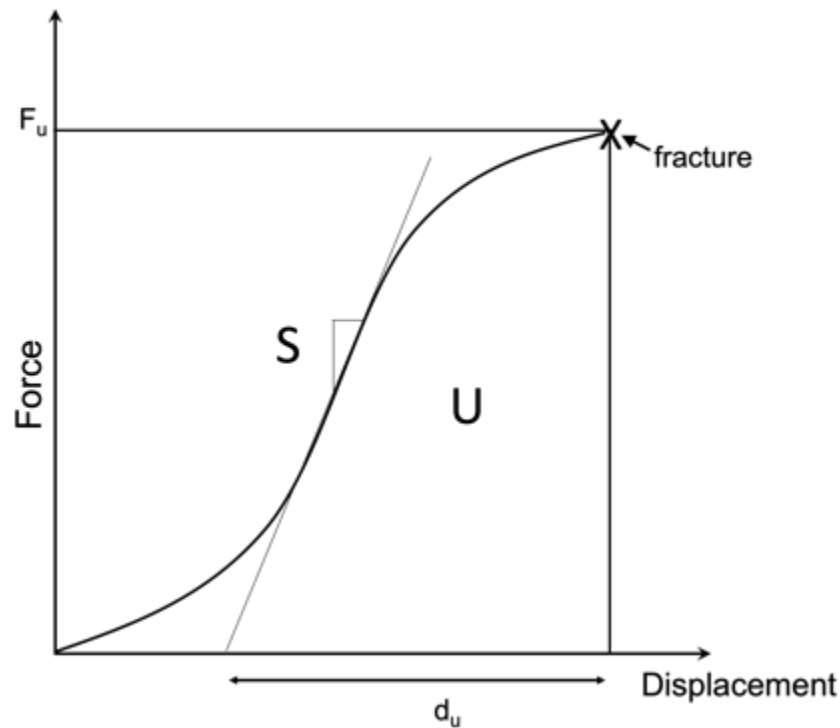
Each of the parameters reflect a different bone property. The ultimate force (F_u) signifies the general integrity of the overall bone structure. The work to failure parameter (U) is the amount of energy needed in order to break a bone and the ultimate displacement (d_u) is inversely proportional to the brittleness of a bone (Turner, 2006).

Mechanical Properties of Cortical Bone

Human cortical bone is anisotropic and therefore has many differences in mechanical properties. For example, cortical bone in long bones is stronger and stiffer when loaded longitudinally along the sagittal plane compared to the transverse plane, indicating that cortical bone can be treated as transversely isotropic. Also, cortical bone is stronger in compressional forces than compared to a tensile force (Turner, 2006). Similarly, the stiff flat bones of the cranium have anisotropic properties comparable to those from the diaphyses of long bones (Peterson and Dechow, 2002).

Figure 4

Bone's Load-Displacement Curve. See the Text above for an Explanation of the Curve



The Mechanical Effects of Loading on Bone

Loading rate has a significant effect on the damage accumulation within cortical bone. The mechanical effects of loading on the microscopic morphology of bone significantly impacts resorption and deposition of bone's functional requirements. Specifically, once strain has reached a maximum threshold, new bone must be deposited to counteract the effects of the imposed strain (Currey, 2012). For example, in cortical bone, this process involves deposition or resorption on the periosteal surface. Also, changes in cross-sectional geometry will occur when the strain is high in order to bring the bone back to its optimal strain threshold (Ruimerman et al., 2005). Strains on trabecular bone will also affect changes in the trabecular configuration in order to orient

themselves to best resist the applied forces placed upon them. Generally, bone cells are responsive to mechanical stimuli in the short term. However, if repeated and continuous stimuli ensue it will have a decreasing osteogenic effect over time (Robling and Turner, 2009).

Overuse in loading initiates small microcracks in bone that causes remodeling in the areas experiencing the strain. Generally, two types of discontinuity are observed: diffuse damage at the collagen fibril level and linear microcracks. The two types of discontinuities are possibly due to different mechanical stressors. Diffuse damage is generally observed in tensile forces and microcracks are usually seen in compressive forces. Correspondingly, the repair mechanisms are different with diffuse damage healed through direct mineral deposition and microcracks healed by remodeling (Currey, 2012).

If a strain increases to the point where a microcrack forms, it will proliferate in the bone's matrix and a complex process is initiated. Generally, many microcracks will be deferred into the cement line or sheath surrounding the osteon. The cement line is an area where minimal mineralization occurs and thus promotes the deflection of cracks by providing a less stiff boundary for crack propagation. When the microfracture encounters the cement line around the osteon, it stops the crack. However, in order for a microfracture to continue in length, more surface energy is required when it encounters the cement line. Therefore, in order for crack propagation, more force is required to sustain a crack than if it had not been halted by the cement line. When enough energy is applied, the microcrack will disrupt the structure of the osteon (Kakar and Einhorn, 2009; Mishinski and Ural, 2011). Crack resistance is higher in planes perpendicular to the osteon (Mishinski and Ural, 2011).

CHAPTER III

Trauma Types, Timing of Injuries, and Fractures

This chapter presents terms and concepts used in describing and discussing trauma analysis. The timing and mechanism of injuries, as well as fracture types and patterns of injury, are also discussed. Bone trauma can be classified into categories based on unique fracture characteristics associated with each trauma type.

Timing of Injuries

Timing of injury is important in trauma analysis. Villa and Mahieu (1991) established guidelines for determining appropriate standards for identifying each category. Antemortem injuries are characterized by an osteogenic response where the body attempts to heal an injury prior to death. Perimortem injuries are identified by fracture outlines having obtuse or acute fracture angles, smooth fracture edges, and evidence of peeling or flaking. Postmortem damage is characterized by differences in color among the fracture edges, transverse fracture outlines, right angle fractures, and fracture edges with jagged blunted ends (Villa and Mahieu, 1991).

On a microscopic level, Pechnikova and colleagues (2011) observed that osteon breaks could indicate perimortem and postmortem trauma or postmortem alteration. Pechnikova et al. (2011) found that, in both perimortem and postmortem events, fractures were twice as likely to extend through the osteon as compared to the cement lines and thus were not a basis for determining perimortem from postmortem trauma based on osteon fracture patterns alone.

To identify antemortem and perimortem injuries, a more in-depth discussion on the healing process is beneficial. In the first 24 hours after a fracture, a hematoma forms

at the site of the break. Osteoclasts and osteoblasts proliferate at the injury site and initiate the inflammation response. The first sign of an osteogenic response is porosity at the ends of the fracture due to the activity of osteoclasts resorbing the bone. Osteoblasts then begin to directly deposit woven bone by intramembranous ossification (McKinley et al., 2003). The callus, which forms at the fracture site, will continue to form until the ends reach pre-fracture stability in approximately three to six months. The remodeling process where woven bone is replaced by trabeculae bone, can continue for up to seven years. The specific presence of the resorption and hard callus denotes the injury as antemortem. However, if early resorption is noted, the injury may be identified as occurring close to the time of death, but a definitive time frame cannot be given as individual response to injury can vary depending upon age, location of the fracture, overall health, and activity level (Martin et al., 2004).

Perimortem injuries occur at, near, or around the time of death and do not show any evidence of healing (Wheatley, 2008; Wendel and Galloway, 2014). A common characteristic of perimortem bone fractures are sharp edges, butterfly fractures, and diagonal fracture angles along the Z-axis (Villa and Mahieu 1991; Wheatley, 2008; Byers, 2017).

Similarly, postmortem trauma manifests as damage unlike the previously discussed antemortem and perimortem trauma. Quatrehome and Iscan (1997) noted features of the external environment, such as soil moisture, sunlight, and animal activity, that can influence the appearance of skeletal material. Weathering can produce longitudinal cracks in the bone parallel to osteon orientation and thus differ from oblique or transverse fractures seen in some trauma cases. Dry bones are much more brittle than

fresh bone and will splinter and break in jagged patterns with break angles that appear to be at 90-degree angles (Villa and Mahieu, 1991).

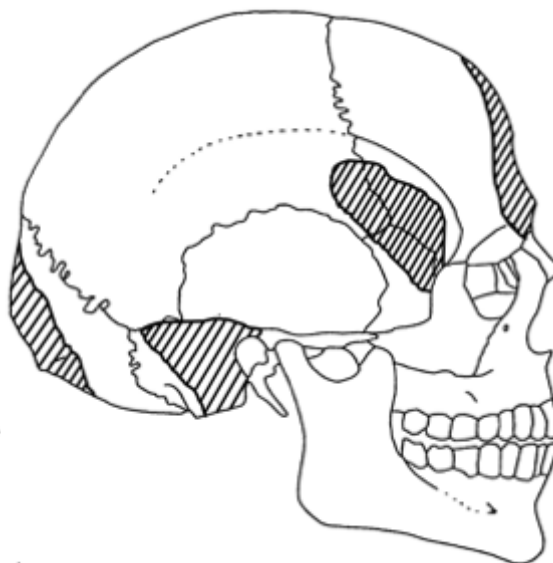
Blunt Force Trauma

Bone trauma can be classified into categories based on unique fracture characteristics associated with each trauma type. Blunt force trauma is characterized as an injury or wound resulting from a blow from a broad or blunt instrument (Byers, 2017). For example, blunt instruments may include a baseball bat, hammer, fist, or pipe. The forces present in this type of trauma can be characterized as direct, crushing, acceleration-deceleration, or sharp blunt impact. The loads experienced in blunt force trauma range from low or high. The mechanical properties of blunt force trauma will vary due to the size and shape of the weapon, the amount of force, and age of the individual. Determining the location, length, width, shape, and fracture type are key characteristics in analyzing blunt force trauma (Kimmerle and Baraybar, 2008).

Cranial blunt force trauma may be represented by depressed, radiating, comminuted, blowout, or basilar fractures (Wedel and Galloway, 2014; Byers, 2017). Depressed fractures cause inward bending of the bone away from the direction of the applied force of impact. These fractures may also be observed as peripheral out-bending depending on the force applied. Radiating fractures occur at the point of impact and move through areas of thinner bone that have less skeletal buttressing. Similarly, if increased force is applied to the skull, concentric fractures may circumscribe the impact site (Hart, 2005; Blau, 2017; Byers, 2017).

Fracture tolerance in cranial bone varies across the skull due to different composition among the bones (Fenton et al., 2005). In general, skull fractures follow

areas of weakness and terminates at areas of interruption in the bones, such as another fracture or a cranial suture (Fenton et al., 2005). While cranial fractures may occur in any portion of the cranial vault, LeCount and Apfelbach (1920) described six regions of greater cranial thicknesses and vertical arches in the skull where the bones are thicker and stronger compared to other areas. The buttresses are located in the midfrontal, midoccipital, paritosphenoïdal, and parietopetrous portion of the skull (Wendel and Galloway, 2014). Similarly, a study by Berryman and Symes (1998), in an attempt to identify areas prone to fracturing, identified four areas of the cranial vault that were structurally stronger. These four areas, depicted in Figure 5, are the midfrontal, midoccipital, posterior temporal, and anterior temporal (Byers, 2017). Bone located between these regions can bend more easily in a vertical manner (Wendel and Galloway, 2014).

Figure 5*Buttresses of the Cranial Vault*

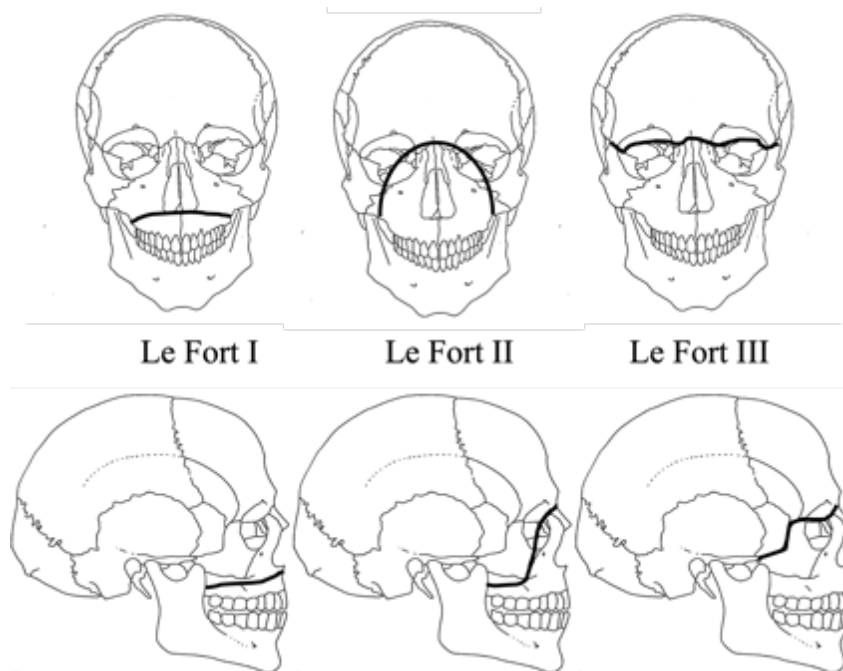
Similarly, Le Fort (1901) described facial buttressing located along the alveolar processes, the malar or zygomatic eminences, and the nasofrontal process of the maxilla (Figure 6). These locations on the facial region are anatomically stronger and resist fracturing. Le Fort identified three types of patterns of facial fracturing based upon the facial buttressing (Figure 7). Specifically, Le Fort I fractures are described as fractures that separate the alveolar portion of the maxilla from the rest of the face. Le Fort II facial fracture pattern is separation of the maxilla with fractures through the maxilla, orbits and bridge of the nose. Le Fort III fractures are described as separation of the skull at the supraorbital margins and zygomatic tripod fractures. Le Fort III fractures are generally associated with fractures occurring on the side of the injury, while Le Fort II type fractures are associated with the opposite side of the injury (Figure 6; Fenton et al., 2005; Wendel and Galloway, 2014).

Figure 6

Buttresses of the Face

**Figure 7**

Le Fort Fracture Types of the Face. See the Text for a Description of each Fracture Type



Typically, the bones of the face can withstand considerable forces when the load is distributed over a wide area. The facial region is supported horizontal and vertical struts. Horizontal struts pass above and below the eye and the hard palate. Vertical struts pass midsagittally along the side of the nose and diagonally from the lateral edge of the hard palate to the lateral edge of the orbit then continues vertically along the orbit. The location of these struts offer resistance to fracturing while the remaining bone tends to crumple upon impact (Wendel and Galloway, 2014).

Ballistic Trauma

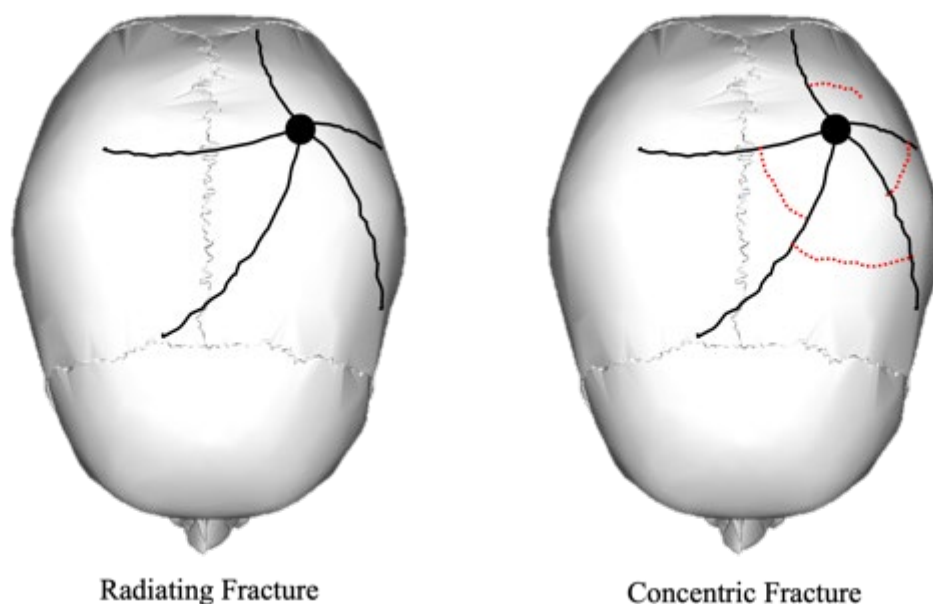
Ballistic trauma results from gunfire projectiles coming into contact with skeletal elements. Projectiles subject bone to sudden, dynamic high-speed stress at a single locus in a bending direction and release a considerable amount of energy within the body (Di Maio, 1999). The compressive force of the bullet often creates a permanent cavity in the bone that can form a variety of morphological shapes such as circular, keyhole, gutter, tangential, or irregular (Di Maio, 1999; Byers, 2017). Wound morphologies and fracture patterns are affected by the size and shape of the projectile, the trajectory of the bullet, velocity, distance of fire, and properties of the affected tissue (Di Maio, 1999). However, in order for a bullet to penetrate bone, the minimum velocity of 60 m/sec is required (Di Maio, 1999).

In gunshot wounds, the deceleration of the bullet when striking the skull causes increased pressure inside the cranial cavity. In the case of close contact gunshot wounds, the skull undergoes an additional source of intracranial pressure, resulting in widespread fracturing of the cranial elements (Di Maio, 1999; Taylor and Kranjoti, 2017). When the bullet is discharged from the muzzle of a gun, gasses are expelled that normally dissipate

into the atmosphere; however, in close contact gunshot wounds the gasses are expelled into the cranial vault, resulting in fractures that generally radiate away from the entrance and exit wounds (Gurdjian et al., 1949; Fenton et al., 2005). Radiating fractures, as seen in Figure 8, radiate or extend away from the entrance location (Di Maio, 1999; Taylor and Kranioti, 2017). In the cranial vault, these lines typically terminate when they encounter a suture or a previous fracture line (Byers, 2017). Similarly, concentric fractures develop perpendicular to the radiating fractures and are produced when the bone is elevated or “heaved” out of the cranial vault from the endocranial pressure (Figure 8; Smith et al., 1987; Berryman and Symes, 1998; Kimmerle and Baraybar, 2008).

Figure 8

Depictions of Radiating and Concentric Fractures on the Cranium Resulting from a Gunshot Wound



Note. The round circle represents the bullet hole in the cranium, while the black lines represent radiating fractures and the red dotted lines denote concentric fractures.

Bullets capable of entering the skull typically have enough remaining energy to perforate through the opposite side of the cranium or become arrested without exiting (Di Maio, 1999). Perforating wounds are described as having both an entrance wound and an exit wound, with the exit wound typically larger than the entrance. Penetrating wounds are described as those that enter the body but do not exit (Di Maio, 1999). This is commonly associated with early destabilization of the bullet and is dependent upon the caliber of the bullet, location of the entrance wound, and distance of the gun when fired (Stephanopoulos et al., 2015).

Using mCT techniques, I tested the null hypothesis (H_0) that suture separation will not differ between trauma types and control specimens on six human bone trauma cases (three ballistic, three blunt force) and three control specimens. Specifically, I tested for the presence and distribution of diastatic fractures along the coronal suture in each case of skeletal trauma to determine if abnormalities in these structures exist. I predicted that sutural separation and diastatic fracture distributions would only be present in the cranial sutures in closest proximity to the trauma site. Also, I tested for asymmetrical separation in the coronal sutures to determine if significant differences could be detected between the sides that received traumatic forces versus the contralateral regions. The occurrence of abnormalities may relate to the direction and distance of the force that caused the trauma. The purpose of this study was to determine how different types of trauma affected adult cranial sutures. This research could provide additional evidence to reconstruct death histories of relatively incomplete skulls with suspected ballistic trauma or blunt force trauma when wounds are not present due to inadequate recovery from a crime scene or animal scavengers.

Research Hypothesis / Objectives***H₀: Hypothesis***

Suture separation in crania that have incurred trauma will not vary from those that have not incurred trauma.

H_A: Hypothesis

Suture separation in crania that have incurred trauma vary from skulls that have not incurred trauma.

H_{A1}: Hypothesis

Sutural separation and diastatic fracture distributions would be statistically greater in skulls that have incurred ballistic trauma than skulls that incurred blunt force trauma.

H_{A2}: Hypothesis

Asymmetrical separation would be statistically greater on the side that received traumatic forces versus the contralateral.

CHAPTER IV

Materials and Methods

Cranial sutures were examined and compared among six human bone trauma cases and three control specimens housed at Southeast Texas Applied Forensic Science Facility (STAFS) in Huntsville, Texas and the Forensic Anthropology Center at Texas State (FACTS) in San Marcos, Texas. STAFS and FACTS are willed body donation facilities where human cadavers are studied as they decompose outside under natural conditions in an environment comprised of pine trees, herbaceous plants, and a humid subtropical climate for teaching and scientific purposes (Hyde et al., 2013). Cadavers used in this study were placed in a supine position on the ground without clothing and a ½” x ½” galvanized wire mesh “cage” was placed over the bodies to protect them from scavengers. Cadavers were allowed to decompose naturally until they reached the skeletonization stage when 50% of the skeleton had been exposed (Langley and Tersigni-Tarrant, 2017). Specimens were then carefully recovered and macerated to remove any remaining soft tissue from the skeletal elements. The maceration process entailed soaking the fleshed bones in water at a constant temperature of 100°C for two 12-hour shifts. Forceps and a hand brush were used to remove any remaining soft tissue. The bones were placed on a metal tray and allowed to dry for two weeks. Each specimen included in this study was identified by their respectively assigned STAFS or FACTS case number to insure the privacy and confidentiality of the individual.

The bones and trauma examined were three crania with intra-oral gunshot wounds, three crania with blunt force trauma, and three crania with no trauma that served as negative controls (Figures 9-17).

Figure 9

Control Specimen, STAFS 2011-005



Figure 10

Control Specimen, FACTS 2013-016



Figure 11

Control Specimen, FACTS 2015-007



Figure 12

Blunt Force Trauma Specimen, STAFS 2014-012



Figure 13

Blunt Force Trauma Specimen, FACTS 2011-022

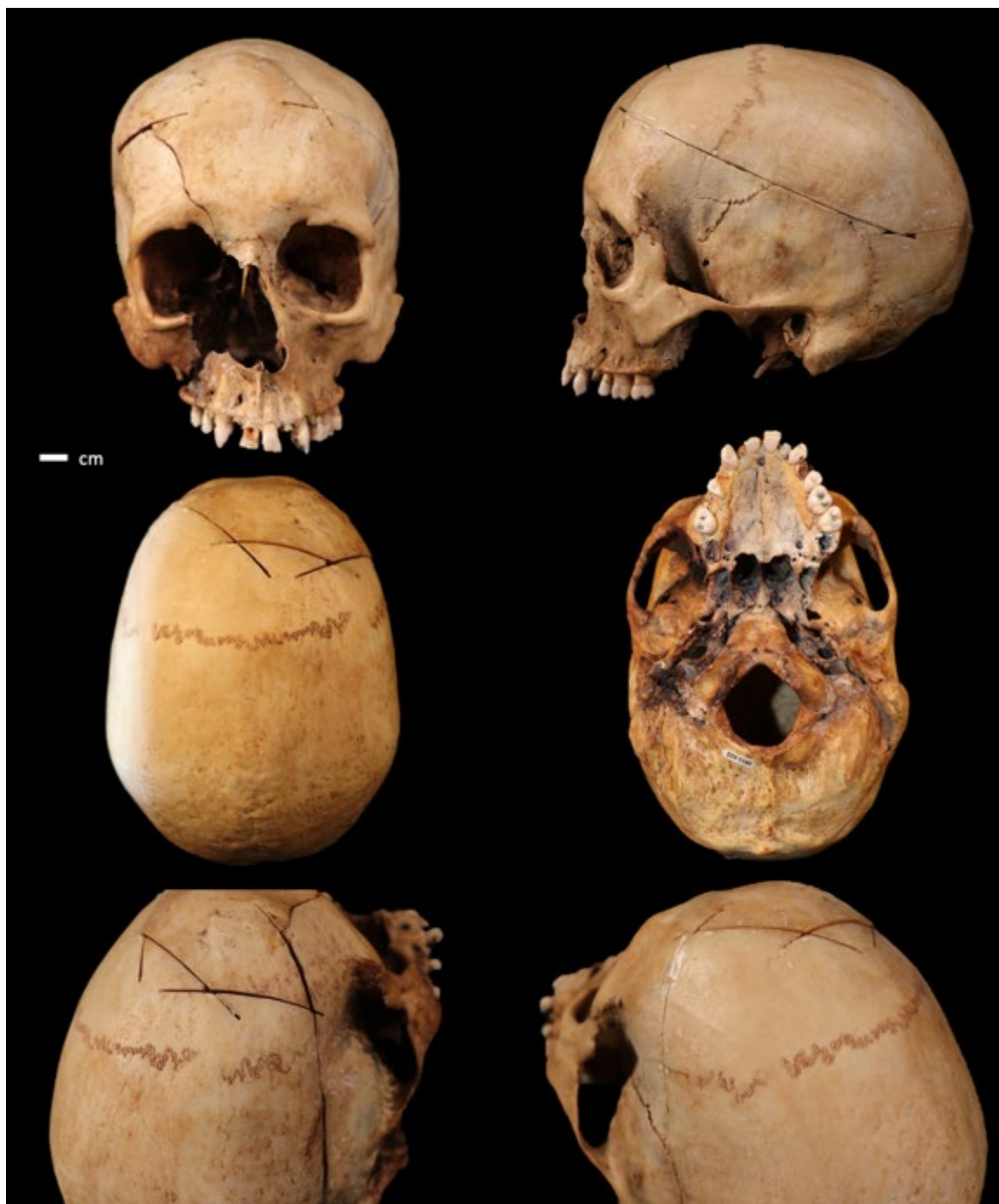


Figure 14

Blunt Force Trauma Specimen, FACTS 2013-057



Figure 15

Intra-Oral Gunshot Wound Specimen, STAFS 2017-017



Figure 16

Intra-Oral Gunshot Wound Specimen, FACTS 2013-046



Figure 17

Intra-Oral Gunshot Wound Specimen, FACTS 2013-019



All specimens were males of European ancestry and ≥ 53 years of age. All cranial injuries were located on one side of the skull and did not directly impact the coronal suture (Table 1).

Table 1

Age of Specimens, Manner of Death, and Side of Trauma for Cranial Examined in this Study

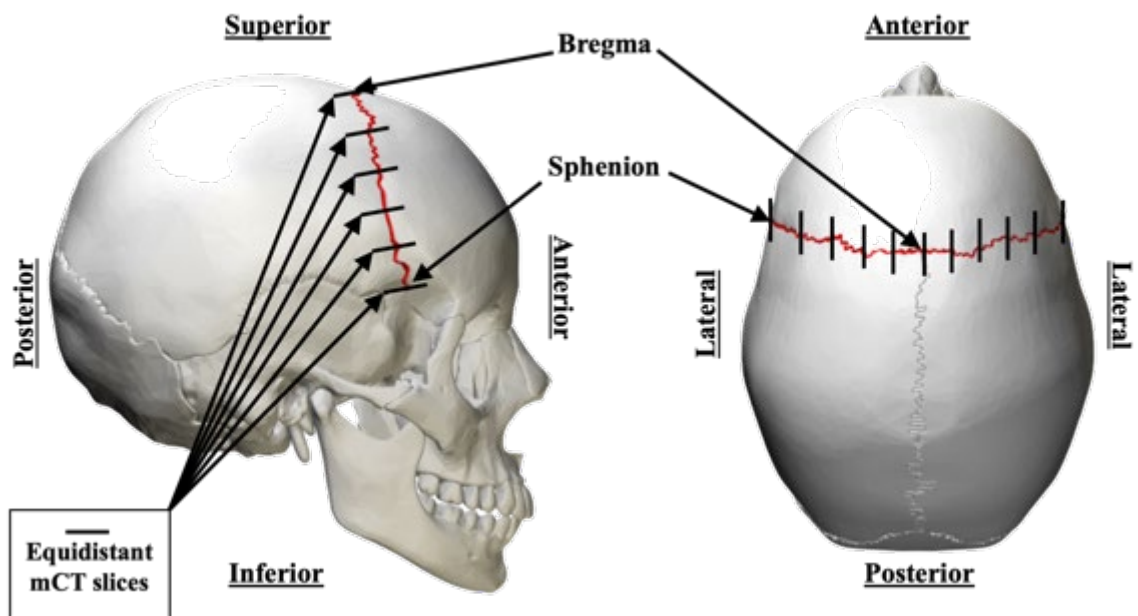
Specimen	Age	Manner of Death	Side of Cranial Trauma
Control			
STAFS 2011-005	53	n/a	n/a
FACTS 2013-016	57	n/a	n/a
FACTS 2015-007	56	n/a	n/a
BFT*			
STAFS 2014-012	59	Accidental	Right
FACTS 2011-022	56	Accidental	Right
FACTS 2013-057	54	Homicide	Left
GSW*			
STAFS 2017-017	53	Suicide	Left
FACTS 2013-046	55	Suicide	Right
FACTS 2013-019	60	Suicide	Left

Note. *BFT = Blunt Force Trauma; GSW = Gunshot Wound.

Cranial specimens were scanned at the University of Texas at Austin High-Resolution X-ray Computed Tomography Facility and Texas State University's Forensic Anthropology Center using NorthStar High-Resolution X-ray CT with voxel size dimensions of 49.4 μm . For standardization of data collection, Type-1 landmarks were used with imaging of the coronal sutures beginning at their origin at the anterior margin of the sphenoparietal suture (sphenion) and terminating at the intersection with the sagittal suture (bregma) (Figure 18).

Figure 18

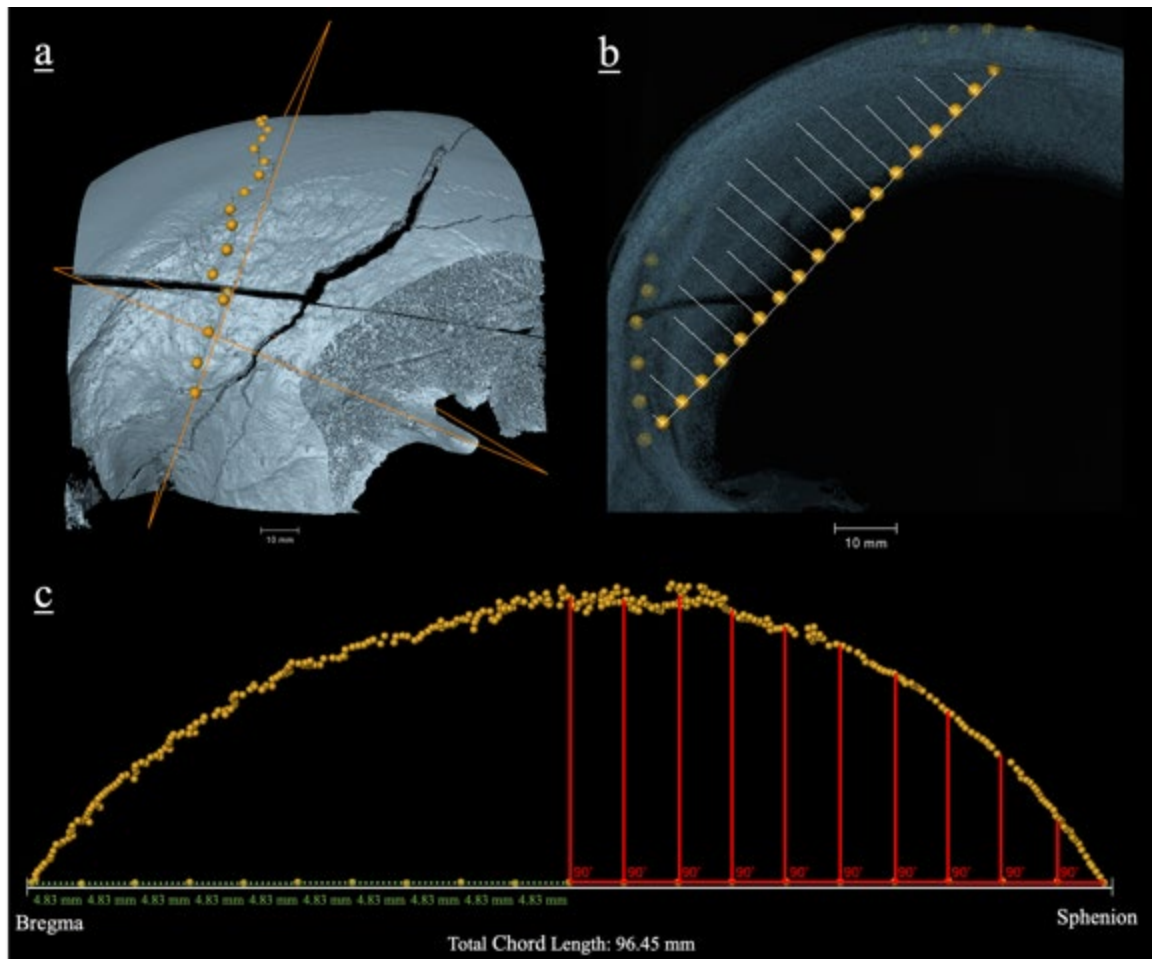
Imaging of the Right and Left Sides of the Coronal Suture



Due to the tortuous nature of the coronal suture, a comb-based approach was used to standardize sampling sites. Utilizing Avizo (v. 9.7.0, Thermo Scientific) segmenting software, a chord line between the bregma and sphenion landmarks was first defined and measured, which allowed for the placement of 20 and 50 equidistant sampling sites along the suture at orthogonal angles from the chord (Table 2; Figure 19). The 20 and 50 equidistant sampling sites were then down-sampled to include an additional 10 and 25 equidistant sampling sites along the coronal suture.

Table 2*Left And Right Chord Lengths from Bregma to Sphenion and Distance between**Landmarks for each of the Crania Scanned*

Specimen	Bregma to Sphenion Chord Length	Landmarks			
		10	20	25	50
<u>mm</u>					
Control					
2011-005 Left	95.64	9.56	4.75	3.83	1.91
2011-005 Right	95.71	9.57	4.77	3.83	1.91
2013-016 Left	97.65	9.77	4.88	3.91	1.95
2013-016 Right	100.59	10.06	5.03	4.02	2.01
2015-007 Left	100.91	10.09	5.05	4.04	2.02
2015-007 Right	98.86	9.89	4.94	3.95	1.98
BFT					
2014-012 Left	100.25	10.03	5.01	4.01	2.01
2014-012 Right	107.81	10.78	5.39	4.31	2.16
2011-022 Left	94.31	9.43	4.72	3.77	1.89
2011-022 Right	91.49	9.15	4.57	3.66	1.83
2013-057 Left	97.37	9.74	4.87	3.89	1.95
2013-057 Right	89.54	8.95	4.48	3.58	1.79
GSW					
2017-017 Left	95.51	9.55	4.78	3.82	1.91
2017-017 Right	96.45	9.65	4.82	3.86	1.93
2013-046 Left	94.90	9.49	4.75	3.80	1.90
2013-046 Right	85.23	8.52	4.26	3.41	1.70
2013-019 Right	100.50	10.05	5.03	4.02	2.01
2013-019 Left	100.42	10.04	5.02	4.02	2.01

Figure 19*Comb-Based Sampling Approach to Standardize Sampling Sites*

Note. a) chord and orthogonal CT slice planes; b) comb-based sampling approach; c) total chord length and orthogonal equidistant sampling sites along the coronal suture.

ImageJ was then used to calculate the total area of separation for individual scan slices at each sampling site and asymmetry was determined by comparing the mean differences in coronal suture separation between sides delineated by bregma (Figure 20). The total coronal sutural areas were calculated and compared between the right and left sides (Table 3, Table 4).

Figure 20

Total Sutural Area at Sampling Site

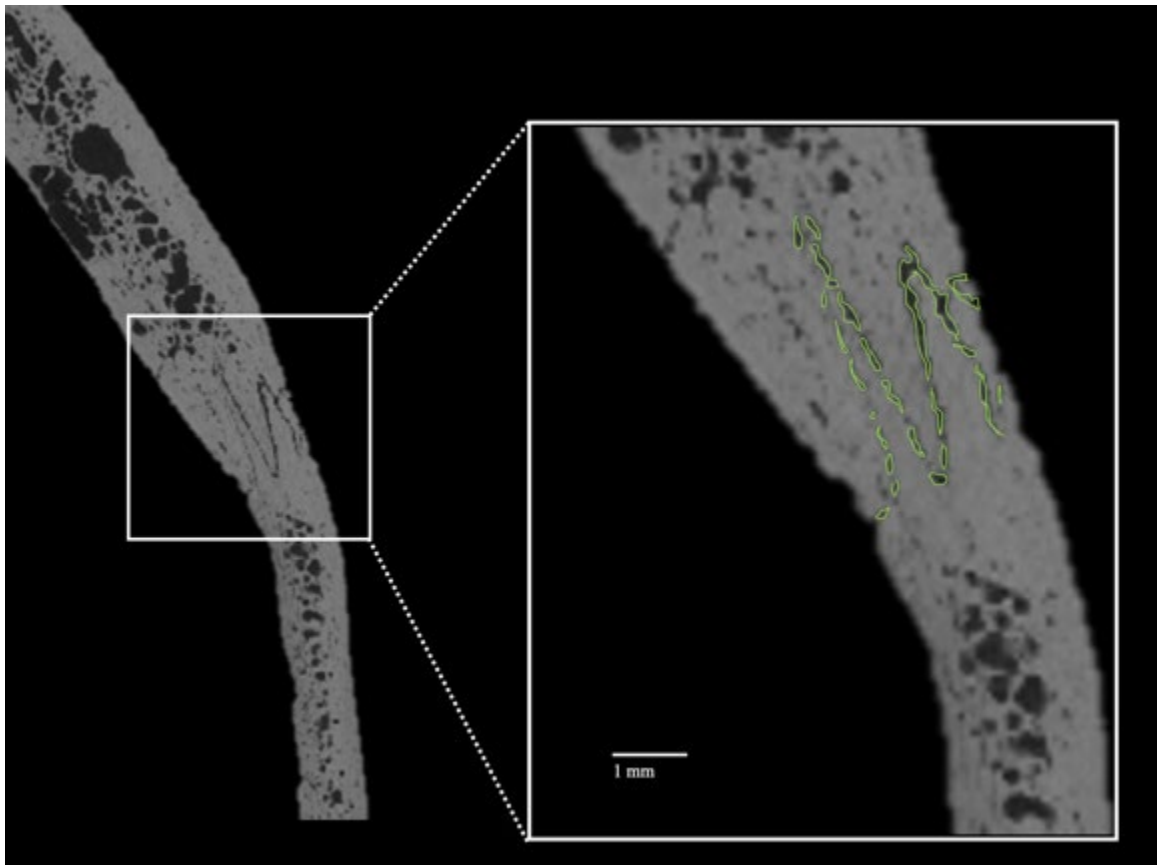


Table 3

Summed Total Area of Complete Coronal Suture Separation using 10, 20, 25, and 50

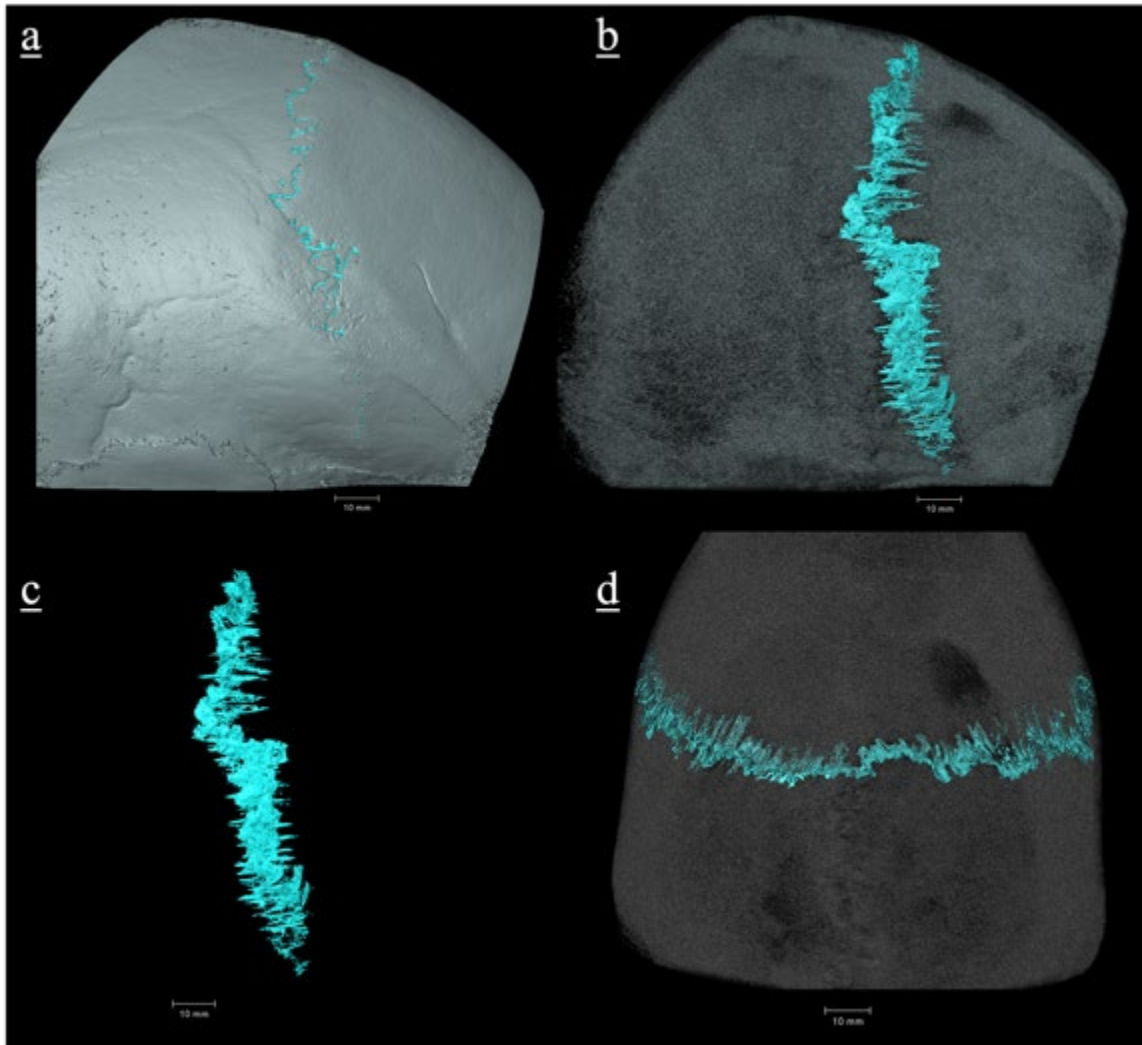
Landmarks

Specimen	Landmarks			
	10	20	25	50
	<u>Summed total area (mm²)</u>			
Control				
STAFS 2011-005	51.120	105.036	94.770	197.535
FACTS 2013-016	39.567	74.829	151.829	290.371
FACTS 2015-007	52.408	109.541	101.160	207.536
BFT				
STAFS 2014-012	75.123	153.003	171.484	343.299
FACTS 2011-022	29.830	62.238	56.002	106.785
FACTS 2013-057	33.615	59.302	63.866	132.780
GSW				
STAFS 2017-017	29.575	62.056	68.975	142.563
FACTS 2013-046	17.809	39.339	64.521	135.213
FACTS 2013-019	10.308	21.571	12.191	24.045

Table 4*Total Area of Left and Right Coronal Suture Separation Per Specimen*

Specimen	Landmarks			
	10	20	25	50
	<u>Total area sum (mm²)</u>			
Control				
2011-005 Left	23.73	47.40	43.25	91.96
2011-005 Right	27.39	57.64	51.516	105.579
2013-016 Left	17.78	33.67	72.41	139.37
2013-016 Right	21.79	41.16	79.421	151.003
2015-007 Left	22.07	48.14	48.62	97.57
2015-007 Right	30.34	61.40	52.544	109.968
BFT				
2014-012 Left	31.840	78.225	63.381	127.039
2014-012 Right	43.283	74.778	108.103	216.260
2011-022 Left	16.125	33.196	30.433	57.968
2011-022 Right	13.705	29.042	25.569	48.817
2013-057 Left	16.207	28.284	26.005	58.596
2013-057 Right	17.408	31.018	37.861	74.184
GSW				
2017-017 Left	15.973	30.548	41.512	89.487
2017-017 Right	13.602	31.508	27.463	53.076
2013-046 Left	10.405	21.577	31.368	66.572
2013-046 Right	7.404	17.762	33.153	68.641
2013-019 Left	2.577	6.330	4.971	10.895
2013-019 Right	10.405	21.577	31.368	66.572

Additionally, Avizo segmenting software was used to segment the complete cranial suture and total sutural volume was calculated using in program measuring tools for each specimen (Figure 21).

Figure 21*View of Segmented Suture*

Note. a) Ectocranial view of segmented suture with crania; b) Ectocranial view of segmented suture with transparent crania; c) Segmented suture without crania; d) view of complete segmented suture.

Bilateral asymmetry in individual specimens was first determined by comparing the total suture area diastasis per slice using a paired t-test. Next, A one-way ANOVA was used to determine if there are significant differences between the traumatized and control crania using the summed total open sutural area. Following this, the average of

the left and right control specimen's sutural diastasis was calculated and tested against the sides with and without trauma using one-way ANOVAs. Finally, a two-way repeated measures ANOVA was used to compare trauma types and side with trauma versus no trauma. All tests were run using the 10, 20, 25, and 50 landmark sampling strategies.

CHAPTER V

Results

The total open sutural areas of the 10, 20, 25, and 50 landmarks were calculated, and a paired t-test was applied to compare differences between the left and right sides of each crania (Table 5-8).

Table 5

Total Left and Right Sutural Areas with 10 Landmarks

Specimen	Left Suture	Left Sutural Range	Right Suture	Right Sutural Range	T-value (Paired)	P-value
	<u>Area (mm²)</u>					
Control						
STAFS 2011-005	2.373	4.194	2.739	4.452	-0.685	0.510
FACTS 2013-016	1.778	3.626	2.179	4.555	-3.007	<i>0.014</i>
FACTS 2015-007	2.207	6.018	3.034	8.020	-1.213	0.256
BFT						
STAFS 2014-012	3.184	8.124	4.328	8.162	-1.412	0.192
FACTS 2011-022	1.613	3.667	1.371	2.486	0.677	0.516
FACTS 2013-057	1.621	3.097	1.741	4.541	-0.300	0.771
GSW						
STAFS 2017-017	1.597	4.283	1.360	3.638	0.512	0.621
FACTS 2013-046	1.041	1.901	0.740	1.899	1.865	0.095
FACTS 2013-019	0.773	2.695	0.258	1.008	2.235	0.052

Note. Significant results are indicated in bold italics.

Table 6*Total Left and Right Sutural Areas with 20 Landmarks*

Specimen	Left Suture	Left Sutural Range	Right Suture	Right Sutural Range	T-value (Paired)	P-value
<u>Area (mm²)</u>						
Control						
STAFS 2011-005	2.370	5.415	2.882	4.642	-1.430	0.169
FACTS 2013-016	1.683	3.626	2.058	4.606	-4.320	<0.001
FACTS 2015-007	2.400	7.503	3.032	8.020	-1.519	0.144
BFT						
STAFS 2014-012	3.911	9.060	3.739	8.182	0.283	0.780
FACTS 2011-022	1.660	3.667	1.452	3.030	0.922	0.368
FACTS 2013-057	1.414	3.097	1.551	4.541	-0.566	0.578
GSW						
STAFS 2017-017	1.527	4.283	1.575	7.024	-0.141	0.889
FACTS 2013-046	1.079	2.309	0.889	3.012	1.323	0.202
FACTS 2013-019	0.762	3.583	0.317	1.118	2.196	0.041

Note. Significant results are indicated in bold italics.

Table 7*Total Left and Right Sutural Areas with 25 Landmarks*

Specimen	Left Suture	Left Sutural Range	Right Suture	Right Sutural Range	T-value (Paired)	P-value
<u>Area (mm²)</u>						
Control						
STAFS 2011-005	1.730	4.400	2.016	4.202	-1.591	0.125
FACTS 2013-016	2.896	7.558	3.177	5.928	-1.102	0.281
FACTS 2015-007	1.945	4.857	2.102	4.096	-0.805	0.429
BFT						
STAFS 2014-012	2.535	5.537	4.324	9.921	-3.595	<i>0.001</i>
FACTS 2011-022	1.217	2.310	1.023	2.592	1.374	0.182
FACTS 2013-057	1.040	2.338	1.514	3.739	-2.292	<i>0.031</i>
GSW						
STAFS 2017-017	1.660	3.487	1.099	3.279	2.666	<i>0.014</i>
FACTS 2013-046	1.254	2.494	1.326	4.136	-0.361	0.722
FACTS 2013-019	0.289	1.002	0.199	0.567	1.633	0.116

Note. Significant results are indicated in bold italics.

Table 8*Total Left and Right Sutural Areas with 50 Landmarks*

Specimen	Left Suture	Left Sutural Range	Right Suture	Right Sutural Range	T-value (Paired)	P-value
<u>Area (mm²)</u>						
Control						
STAFS 2011-005	1.839	4.981	2.111	4.215	-1.904	0.063
FACTS 2013-016	2.787	7.632	3.020	5.851	-1.258	0.214
FACTS 2015-007	1.951	4.890	2.200	4.033	-1.965	0.055
BFT						
STAFS 2014-012	2.541	6.061	4.325	9.921	-4.679	<0.001
FACTS 2011-022	1.159	2.179	0.976	2.539	2.070	0.044
FACTS 2013-057	1.172	2.304	1.484	3.688	-2.403	0.020
GSW						
STAFS 2017-017	1.790	3.756	1.062	3.297	5.075	<0.001
FACTS 2013-046	1.331	3.240	1.372	5.859	-0.286	0.776
FACTS 2013-019	0.263	1.002	0.218	0.873	1.246	0.219

Note. Significant results are indicated in bold italics.

The results for paired t-test using the 10 landmarks sampling sites of the crania indicate that only control specimen 2013-016 had significant differences ($p \leq 0.05$) between the right and left sides (Table 5). The right coronal suture sum area was 2.179 mm² and the left side mean sutural area was 1.778 mm².

Results for the 20 landmark sampling sites indicate that only GSW 2013-019 specimen had a statistically significant difference between the right and left sides of the coronal suture in the intraoral gunshot wound and blunt force trauma specimens (Table 6). The right coronal suture sum area was 0.317 mm² and the left side sum sutural area was 0.762 mm². One control cranium (2013-016) exhibited significant differences between the right and left sides.

The results for the 25 landmark sampling sites revealed that three trauma crania, BFT 2014-012, BFT 2013-057, and GSW 2017-017, exhibited significant differences between the right and left sides for the coronal suture (Table 7). The BFT 2014-012 right coronal suture sum area was 4.324 mm² and the left sum sutural area was 2.535 mm²; the BFT 2013-057 right coronal suture sum area was 1.514 mm² and the left sum sutural area was 1.040 mm²; and the GSW 2017-017 GSW right coronal suture sum was 1.099 mm² while the left sutural sum was 1.660 mm².

The 50 landmark sampling site results indicated that four crania had significant differences between the right and left sides of the suture (Table 8). All three BFT specimens (2014-012, 2011-022, 2013-057) and one intraoral GSW specimen (2017-017) exhibited differences in the sum sutural area between the sides of the coronal suture. BFT 2014-012 exhibited highly significant differences between sides ($p < 0.001$) with the right sutural sum of 4.325 mm², while the left sutural sum was 2.541 mm²; BFT 2011-022's right sutural sum area was 0.976 mm², while the left sum area was 1.159 mm²; and BFT 2013-057's right sutural sum area was 1.484 mm² and the left was 1.172 mm². Lastly, GSW specimen 2017-017 exhibited highly significant differences between sides ($p < 0.001$), with the right sutural sum 1.373 mm² and left sutural sum 1.331 mm², respectively.

A one-way ANOVA was then performed to compare total coronal sutural diastasis among groups using 10, 20, 25 and 50 landmarks (Table 9).

Table 9*One-Way Anova Comparing Total Sum of Sutural Separation among Groups*

# of Landmarks	SS	df	F	P-value	Kruskal-Wallace H (chi2)	p-value
10 Landmarks						
Between Groups	1539.450	2	2.977	0.127	5.600	0.061
Within Groups	1551.550	6				
20 Landmarks						
Between Groups	5655.420	2	2.353	0.176	4.622	0.099
Within Groups	7211.750	6				
25 Landmarks						
Between Groups	7248.110	2	1.771	0.249	2.756	0.252
Within Groups	12275.400	6				
50 Landmarks						
Between Groups	27399.600	2	1.725	0.256	2.756	0.252
Within Groups	47657.300	6				

The results of the one-way ANOVA comparing total sum of sutural separation among groups did not reveal any statistically significant results.

One-way ANOVAs were performed to compare total sutural area averages of the control specimens with the areas of the side with trauma (Table 10) and side without trauma (Table 11).

Table 10

One-Way Anova with Total Average Sum of Control Specimens and Total Area of Side with Trauma

# of Landmarks	SS	df	Mean Square	F	P-value	Kruskal-Wallace H (chi2)	p-value
10 Landmarks							
Between Groups	378.825	2	189.412	1.862	0.235	4.622	0.099
Within Groups	610.229	6	101.705				
20 Landmarks							
Between Groups	1271.54	2	635.772	2.204	0.192	3.822	0.148
Within Groups	1730.89	6	288.481				
25 Landmarks							
Between Groups	1635.12	2	817.558	0.869	0.466	2.756	0.252
Within Groups	5645.45	6	940.909				
50 Landmarks							
Between Groups	6103.97	2	3051.99	0.830	0.481	2.756	0.252
Within Groups	22075.7	6	3679.29				

Table 11

One-Way Anova with Total Average Sum of Control Specimens and Total Area of Contralateral Side of Trauma

# of Landmarks	SS	df	Mean Square	F	P-value	Kruskal-Wallace H (chi2)	p-value
10 Landmarks							
Between Groups	396.053	2	198.027	4.917	0.054	5.600	0.061
Within Groups	241.644	6	40.274				
20 Landmarks							
Between Groups	1574.680	2	787.342	2.460	0.166	4.622	0.099
Within Groups	1920.120	6	320.020				
25 Landmarks							
Between Groups	2056.130	2	1028.070	4.134	0.074	5.067	0.079
Within Groups	1491.990	6	248.665				
50 Landmarks							
Between Groups	7950.530	2	3975.260	4.263	0.070	5.067	0.079
Within Groups	5594.600	6	932.433				

Results of the one-way ANOVAs comparing total sutural area averages of the control specimens with the areas of the side with trauma and side without trauma total did not reveal any statistically significant results.

Finally, a two-way repeated measures ANOVA was performed comparing trauma type sutural separation areas and side using the 10, 20, 25, and 50 landmarks (Table 12).

Table 12*Two-Way Repeated Measures Anova Comparing Trauma Types and Side*

# of Landmarks	SS	df	Mean square	F	p-value
10 Landmarks					
Trauma Type	272.539	1	272.539	0.693	0.443
Side	6.35099	1	6.351	0.825	0.406
Trauma Type x Side	0.4532	1	0.453	0.051	0.830
20 Landmarks					
Trauma Type	957.316	1	957.316	0.583	0.480
Side	1.60115	1	1.601	0.256	0.634
Trauma Type x Side	8.72541	1	8.725	1.807	0.237
25 Landmarks					
Trauma Type	884.092	1	884.092	0.420	0.546
Side	88.4973	1	88.497	0.878	0.392
Trauma Type x Side	4.09847	1	4.098	0.035	0.859
50 Landmarks					
Trauma Type	3291.07	1	3291.070	0.381	0.564
Side	461.267	1	461.267	1.186	0.326
Trauma Type x Side	23.4986	1	23.499	0.049	0.833

The results of the two-way repeated measures ANOVA comparing trauma types and side did not reveal any statistically significant results using 10, 20, 25, or 50 landmarks.

A one-way ANOVA was then performed to compare total coronal sutural diastasis among groups using total sutural volumes (Table 13).

Table 13*One-Way Anova Results Comparing Total Volume among Specimens*

Total Sutural Volume	SS	df	Mean Square	F	P-value	Kruskal-Wallace H (chi2) p-value	
Between Groups	226569	2	113284	2.788	2.788	5.6	0.061
Within Groups	243805	6	40634.1				

The results of the one-way ANOVA comparing total volume of sutural separation among groups did not reveal any statistically significant results.

Next, one-way ANOVAs were performed to compare total sutural volumes of the control specimens with the areas of the side with trauma (Table 14) and side without trauma (Table 15).

Table 14*One-Way Anova with Average Sum of Control Specimen Volume and Side of Trauma*

Total Sutural Volume	SS	df	Mean Square	F	P-value	Kruskal-Wallace H (chi2) p-value	
Between Groups	58743.2	2	29372	1.889	0.231	3.2	0.202
Within Groups	93306.2	6	15551				

Table 15*One-Way Anova with Average Sum of Control Specimen Volume and Side of No Trauma*

Total Sutural Volume	SS	df	Mean Square	F	P-value	Kruskal-Wallace H (chi2) p-value	
Between Groups	56366.3	2	28183	4.511	0.064	3.2	0.202
Within Groups	37486.8	6	6248				

Results of the one-way ANOVAs comparing total sutural volumes of the control specimens with the areas of the side with trauma and side without trauma total did not reveal any statistically significant results.

Lastly, a two-way repeated measures ANOVA was performed comparing trauma type and side using the sutural volumes (Table 16).

Table 16

Two-Way Repeated Measures Anova Comparing Trauma Type and Side Volumes

Trauma Specimens	SS	df	Mean square	F	p-value
Trauma Type	25676.4	1	25676.4	0.5365	0.4967
Side	821.756	1	821.756	0.7879	0.4154
Trauma Type x Side	1120.34	1	1120.34	1.139	0.3346

The results of the two-way repeated measures ANOVA comparing trauma types and side using the sutural volumes did not reveal any statistically significant results.

CHAPTER VII

Discussion and Conclusion

From the reported results, the paired t-test showed that side of trauma can be detected in individual specimens. Blunt force trauma specimens 2011-022 and 2013-057 both exhibited smaller total sutural separation on the side that received the trauma whereas specimen 2014-012 exhibited larger total sutural separation on the trauma inflicted side. Both BFT specimens 2014-012 and 2011-022 had similar injuries: trauma was inflicted to the right zygomatic region in BFT specimen 2014-012 and BFT specimen 2011-022 exhibited trauma to the medial aspect of the right zygomatic and nasal bones. However, these two specimens displayed differing sides of sutural separation. These results may be due to the instrument and direction of force used to inflict the trauma. Similarly, it may be due to the individual specimens' degree of sutural closure or individual fracture patterns that were able to dissipate the force of the blow.

When trauma to the skull occurs, fracture lines follow areas of weakness and terminate at areas of interruption in the bones, such as another fracture line or a cranial suture (Byers, 2017; Fenton et al., 2005). Specimen 2011-022 displayed a large radiating fracture on the right superior supraciliary arch that extended to the right frontal eminence. This could be a reason why the sutural separation was smaller on the trauma inflicted side due to the radiating fracture dissipating the energy of the blow. Similarly, direction of trauma for BFT 2013-057 was from the posterior aspect of the left temporal bone and had greater coronal suture separation on the left side with a radiating fracture extending through the left coronal suture. The differences between BFT specimens 2013-057 and 2011-022 the radiating fractures is that 2011-022's fracture terminated before it reached

the coronal suture indicating there may not have been enough energy remaining to cause a pronounced effect on the suture. While specimen 2013-057 radiating fracture extended through the coronal suture potentially resulting in increased energy on the suture.

The results of the paired t-test for the GSW specimens indicated that only specimen 2017-017 exhibited statistically significant differences. The exit wound was located on the anterior portion of the left parietal and displayed greater sutural separation on the trauma inflicted side. GSW specimens 2013-046 and 2013-019 did not exhibit statistically significant differences between sides for the coronal suture but did display larger total sutural separation on the trauma inflicted side. These results may be due to the location of the exit wound and distance from the coronal suture in specimen 2013-019. The exit wound was located on the occipital bone near the foramen magnum and may have been too far from the coronal suture to cause significant sutural diastasis. However, the exit wound 2017-017 was in close proximity to the left coronal suture, which produced highly significant sutural separation ($p < 0.0001$). Similarly, 2013-019 had the lowest total sutural separation on both sides: the coronal and sagittal sutures were completely obliterated on the majority of the ectocranial portion of the cranium. This could also be another reason as to why the results from the paired t-test were not significant. For GSW specimen 2013-046, the cranium was severely fractured into seven fragments with several areas, such as the hard palate, entirely missing. The exit wound was determined to be on the middle aspect of the right parietal. A large radiating fracture posterior to the coronal suture traversed the length of the suture and fractured the frontal bone away from the parietals. It is possible that this large radiating fracture distributed

the energy across the complete suture that resulted in no significant differences between the sides of the cranium.

All three blunt force trauma specimens exhibited significant differences in sutural separation between the sides compared to one intraoral gunshot wound specimen. This may be due to the different amount of loading placed upon the bone from the different trauma types. In blunt force trauma, the loading is considered slow while in ballistic trauma the loading is rapid or fast. In slow loading, the bone takes longer to fail or fracture and will display a greater amount of plastic deformation (Kroman and Symes, 2013). In slow loading, the bone is able to deform to a particular point and at a certain level of force, ultimately returning to its original shape once the load is removed (Iskan and Steyn, 2013). However, if the load is great enough to surpass elastic deformation, the bone will enter plastic deformation resulting in failure or fracture. Due to rapid loading to the cranium in gunshot wounds, bone will experience explosive failure with little to no plastic deformation and will shatter (Berryman and Symes 1998). Therefore, the blunt force trauma specimens displayed a greater amount of plastic deformation, which may be the reason why all three specimens exhibited significant differences in sutural separation. Alternately, the gunshot wound specimens experienced no plastic deformation and the energy from the bullet possibly dissipated in the radiating fractures. Cohen and colleagues (2016) have shown that energy dissipates at fractures using controlled experiments. Again, the location of the injury and age of the individual effects how bone will respond to a particular load (Symes et al., 2012; Galloway, 1999). All the specimens were between the ages of 50 – 60 years of age; however, the age at which the coronal suture begins to fuse or obliterate varies greatly among individuals. Similarly, every

bone, and different areas located in the same bone, will react differently to the stress and strains of loading (Iskan and Steyn, 2013).

Data analyses in this study verified that greater numbers of landmarks used in the comb-based approach provided a more comprehensive analysis of sutural separation in crania. Analyses with 10 and 20 landmarks did yield significant results between the sides of the cranium for control specimen 2013-016; however, differences between sides for 2013-016 were not statistically significant as the number of landmarks increased to 25 and 50. Therefore, increasing the number of landmarks has shown to be a better and more inclusive indicator of sutural separation.

The results from the one-way ANOVA comparing the total sum area of sutural separation among specimens did not yield statistically significant results for the 10, 20, 25, and 50 landmarks or the total sutural volumes (Table 9; Table 13). Therefore, total sutural separation cannot be used to quantify trauma between specimen types examined in this study. Similarly, one-way ANOVAs using the total average sum of the control specimens and analyzing the side of trauma and the contralateral in the specimens were not significant (Tables 10-11) and total sutural volumes (Tables 14-15). Finally, there were no significant results from the two-way repeated measures ANOVA comparing trauma type, side, and both trauma type and side for the specimens examined in this study (Table 12; Table 16). Consequently, the results from these analyses fail to reject my null hypothesis that suture separation in crania that have incurred trauma will not vary from those that have not incurred trauma.

Due to these unexpected results, I further hypothesize that the varying degrees of trauma are difficult to quantify due to the amount of variation and variables exhibited by

the specimens used in this analysis. Specifically, the varying degrees of sutural patency and obliteration, locations of the trauma on the crania, distance of trauma from the coronal suture and unknown ballistic data, and the amount of force used to inflict the blunt force trauma. It should be noted that this study used specimens with real life trauma and thus could not control for most variables.

Future studies with additional intraoral gunshot wound and blunt force trauma specimens are needed to increase the sample size before any generalizations should be made. If possible, these studies should also incorporate data on the projectile itself including the type of weapon used, the caliber of bullet, and composition of the round. Similarly, in blunt force trauma specimens, data on the type of instrument used to inflict the trauma should also be noted. Ideally, controlled trauma experiments should be performed to limit the number of variables associated with this study. Cadaver crania should be mCT scanned before and after the trauma is inflicted to determine the extent of suture separation. While many methods in forensic anthropology rely predominantly on macroscopic observation of the trauma, the methods presented here still have the potential to provide valuable microscopic trauma analyses.

REFERENCES

- Acsadi, Gy., & Nemeskeri, J. (1974). History of human life span and mortality. *Current Anthropology*, 15(4), 495–507. <https://doi.org/10.1086/201508>
- Baker, R. K. (1984). The relationship of cranial suture closure and age analyzed in a modern multi-racial sample of males and females. Master of Arts Thesis, Department of Anthropology, California State University-Fullerton.
- Berryman, H.E. & Symes, S.A., (1998). Recognizing gunshot and blunt cranial trauma through fracture interpretation. In: Reichs, K. *Forensic Osteology: Advances in the Identification of Human Remains*. Springfield: Charles C Thomas Publisher, LTD.
- Blau, S. (2017). How traumatic: A review of the role of the forensic anthropologist in the examination and interpretation of skeletal trauma. *Australian Journal of Forensic Sciences*, 49(3), 261–280. <https://doi.org/10.1080/00450618.2016.1153715>
- Bolk, L. (1917). On metopism. *American Journal of Anatomy*, 22(1), 27–47. <https://doi.org/10.1002/aja.1000220103>
- Byers, S. N. (2017). *Introduction to forensic anthropology*. London; New York: Routledge.
- Sekharan, C. P. (1985). Identification of skull from its suture pattern. *Forensic Science International*, 27(3), 205–214. [https://doi.org/10.1016/0379-0738\(85\)90156-2](https://doi.org/10.1016/0379-0738(85)90156-2)
- Chopra, S. R. K. (1957). The cranial suture closure in monkeys. *Proceedings of the Zoological Society of London*, 128(1), 67–112. <https://doi.org/10.1111/j.1096-3642.1957.tb00257.x>

- Christensen, A. M., Passalacqua, N. V., & Bartelink, E. J. (2014). Age estimation. In *Forensic Anthropology*, 243–284. Elsevier. <https://doi.org/10.1016/B978-0-12-418671-2.00010-0>
- Cohen, M. M. (1993). Sutural biology and the correlates of craniosynostosis. *American Journal of Medical Genetics*, 47(5), 581–616.
<https://doi.org/10.1002/ajmg.1320470507>
- Cohen, H., Kugel, C., May, H., Medlej, B., Stein, D., Slon, V., Hershkovitz, I., & Brosh, T. (2016). The impact velocity and bone fracture pattern: Forensic perspective. *Forensic Science International*, 266, 54–62.
<https://doi.org/10.1016/j.forsciint.2016.04.035>
- Campobasso, C. P., De Micco, F., Bugelli, V., Cavezza, A., Rodriguez, W. C., 3rd, & Della Pietra, B. (2019). Undetected traumatic diastasis of cranial sutures: A case of child abuse. *Forensic Science International*, 298, 307-311.
[10.1016/j.forsciint.2019.03.011](https://doi.org/10.1016/j.forsciint.2019.03.011)
- Corega, C., Vaida, L., Baciut, M., Serbanescu, A., & Palaghita-Banias, L. (2010). Three-dimensional cranial suture morphology analysis. *Romanian Journal of Morphology and Embryology*, 51(1), 123–127.
- Currey, J. D. (2012). The structure and mechanics of bone. *Journal of Materials Science*, 47(1), 41–54. <https://doi.org/10.1007/s10853-011-5914-9>
- De Coster, P. J., Mortier, G., Marks, L. A., & Martens, L. C. (2007). Cranial suture biology and dental development: Genetic and clinical perspectives: Cranial suture biology and dental development. *Journal of Oral Pathology & Medicine*, 36(8), 447–455. <https://doi.org/10.1111/j.1600-0714.2007.00553.x>

- DiMaio, V. J. (1999). *Gunshot wounds: Practical aspects of firearms, ballistics, and forensic techniques*. CRC press.
- Dryden, R. (1978). *Before birth*. London: Heinemann Educational Books.
- Dwight, T. (1890). The closure of the cranial sutures as a sign of age. *The Boston Medical and Surgical Journal*, 122(17), 389–392.
<https://doi.org/10.1056/NEJM189004241221701>
- Fenton, T. W., Stefan, V. H., Wood, L. A., & Sauer, N. J. (2005). Symmetrical fracturing of the skull from midline contact gunshot wounds: Reconstruction of individual death histories from skeletonized human remains. *Journal of Forensic Sciences*, 50(2), 1–12. 10.1520/jfs2004198
- Furuya, Y., Edwards, M. S. B., Alpers, C. E., Tress, B. M., Ousterhout, D. K., & Norman, D. (1984). Computerized tomography of cranial sutures. *Journal of Neurosurgery*, 61(1), 53–58. <https://doi.org/10.3171/jns.1984.61.1.0053>
- Furuya, Y., Edwards, M. S., Alpers, C. E., Tress, B. M., Ousterhout, D. K., & Norman, D. (1984). Computerized tomography of cranial sutures: Part 1: Comparison of suture anatomy in children and adults. *Journal of neurosurgery*, 61(1), 53-58.
- Galloway, A. (1999). *Broken bones: Anthropological analysis of blunt force trauma*. Springfield, Ill: Charles C Thomas.
- Ginter, J. K. (2005). A test of the effectiveness of the revised maxillary suture obliteration method in estimating adult age at death. *Journal of Forensic Science*. 50(6):1303-1309.
- Gruspier, K. L., Mullen, G. J. (1991). Maxillary suture obliteration: A test of the Mann method. *Journal of Forensic Science*. 36(2):512-519.

- Harrison, R. G. (1978). *Clinical embryology: Monographs for students of medicine*. London: Academic Press.
- Hart, G. (2005). Fracture pattern interpretation in the skull: Differentiating blunt force from ballistics trauma using concentric fractures. *Journal of Forensic Sciences*, *50*, 1276–1281. <https://doi.org/10.1520/JFS2004219>
- Hart, N. H., Nimphius, S., Rantalainen, T., Ireland, A., Siafarikas, A., & Newton, R. U. (2017). Mechanical basis of bone strength: Influence of bone material, bone structure and muscle action. *Journal of Musculoskeletal & Neuronal Interactions*, *17*(3), 114–139.
- Harth, S., Obert, M., Ramsthaler, F., Reuß, C., Traupe, H., & Verhoff, M. A. (2009). Estimating age by assessing the ossification degree of cranial sutures with the aid of Flat-Panel-CT. *Legal Medicine*, *11*, S186–S189. <https://doi.org/10.1016/j.legalmed.2009.01.091>
- Hauser, G., & Stefano, G. F. (1989). *Epigenetic variants of the human skull*. Stuttgart: E. Schweizerbart'sche Verlagsbuchhandlung.
- Herring, S. W. (1972). Sutures – a tool in functional cranial analysis. *Acta Anatomica*, *(82)* 222-247.
- Hyde, E. R., Haarmann, D. P., Lynne, A. M., Bucheli, S. R., & Petrosino, J. F. (2013). The living dead: Bacterial community structure of a cadaver at the onset and end of the bloat stage of decomposition. *PLoS ONE*, *8*(10). [10.1371/journal.pone.0077733](https://doi.org/10.1371/journal.pone.0077733)
- Iscan, M. Y., & Steyn, M. (2013). *The human skeleton in forensic medicine, 3rd edition*. Charles C. Springfield, Illinois.

- Iyengar, R. J., Klinge, P. M., Chen, W., Sullivan, S. R., & Taylor, H. O. (2015). Management of craniosynostosis at an advanced age: Clinical findings and interdisciplinary treatment in a 17-year-old with pan-suture synostosis. *Interdisciplinary Neurosurgery*, 2(1), 61–64.
<https://doi.org/10.1016/j.inat.2015.01.003>
- Kakar, S., Little, D., & Einhorn, T. A. (2009). Can we improve fixation and outcomes in the treatment of femoral neck fractures? The use of pharmaceuticals. *Journal of Orthopaedic Trauma*, 23(6), 413–421.
<https://doi.org/10.1097/BOT.0b013e3181ac64a0>
- Kimonis, V., Gold, J.-A., Hoffman, T. L., Panchal, J., & Boyadjiev, S. A. (2007). Genetics of craniosynostosis. *Seminars in Pediatric Neurology*, 14(3), 150–161.
<https://doi.org/10.1016/j.spen.2007.08.008>
- Love, J. (2008). Erin H. Kimmerle, José Pablo Baraybar, Skeletal trauma: Identification of injuries resulting from human rights abuse and armed conflict. *Forensic Science, Medicine, and Pathology*, 4, 202–202. <https://doi.org/10.1007/s12024-008-9048-6>
- Kirmi, O., Lo, S. J., Johnson, D., & Anslow, P. (2009). Craniosynostosis: A radiological and surgical perspective. *Semin Ultrasound CT MR*, 30(6), 492-512.
- Kokich, V. G. (1986). The biology of sutures. In: Cohen, M. M.: *Craniosynostosis: Diagnosis, Evaluation and Management*. New York: Raven Press.
- Kranioti, E. F. (2015). Forensic investigation of cranial injuries due to blunt force trauma: Current best practice. *Research and Reports in Forensic Medical Science* 5, 25–37. <https://doi.org/10.2147/RRFMS.S70423>

- Krogman, W., & Iscan, M. (1986). *The Human Skeleton in Forensic Medicine*.
Springfield, Illinois.
- Kroman, A., & Symes, S. (2013). Investigation of skeletal trauma. *Research Methods in Human Skeletal Biology*, 219–239. <https://doi.org/10.1016/B978-0-12-385189-5.00008-X>
- Langley, N.R., & Tersigni-Tarrant, M.A. (2017). *Forensic Anthropology: A Comprehensive Introduction*, Second Edition. CRC Press.
<https://doi.org/10.4324/9781315300030>
- Langman, J. (1981). *Medical Embryology*, 4th ed. Baltimore: Williams & Wilkins.
- LeCount, E. R., & Apfelbach, C. W. (1920). Pathologic anatomy of traumatic fractures of cranial bones and concomitant brain injuries. *Journal of the American Medical Association*, 74(8), 501. <https://doi.org/10.1001/jama.1920.02620080003002>
- LeFort, R. (1901). *Experimental study of fractures of the upper jaw. Part III*. Rev. Chir. Pris., 23:479-507. Reprinted (1972) in *Plastic Reconstructive Surgery*, 50:600-605.
- Li, S., Abdel-Wahab, A., Demirci, E., & Silberschmidt, V. V. (2013). Fracture process in cortical bone: X-FEM analysis of microstructured models. *International Journal of Fracture*, 184(1–2), 43–55. <https://doi.org/10.1007/s10704-013-9814-7>
- Liu, L., Jiang, Y., Boyce, M., Ortiz, C., Baur, J., Song, J., & Li, Y. (2017). The effects of morphological irregularity on the mechanical behavior of interdigitated biological sutures under tension. *Journal of Biomechanics*, 58, 71—78.
<https://doi.org/10.1016/j.jbiomech.2017.04.017>

- Maloul, A., Fialkov, J., & Whyne, C. M. (2013). Characterization of the bending strength of craniofacial sutures. *Journal of Biomechanics*, *46*(5), 912–917.
<https://doi.org/10.1016/j.jbiomech.2012.12.016>
- Maloul, A., Fialkov, J., Hojjat, S. P., & Whyne, C. M. (2010). A technique for the quantification of the 3D connectivity of thin articulations in bony sutures. *Journal of Biomechanics*, *43*(6), 1227–1230.
<https://doi.org/10.1016/j.jbiomech.2009.11.024>
- Mann, R. W., Jantz, R. L., Bass, W. M., Willey, P. S. (1991). Maxillary suture obliteration: A visual method for estimating skeletal age. *Journal of Forensic Science*. *36*(3):781-91.
- Martin R. B., Burr D. B., Sharkey N. A. (1998) Mechanical Properties of Bone. In: *Skeletal Tissue Mechanics*. Springer, New York, NY.
- McKinley, T. O., English, D. K., & Bay, B. K. (2003). Trabecular bone strain changes resulting from partial and complete meniscectomy. *Clinical Orthopaedics and Related Research*, *407*, 259–267. <https://doi.org/10.1097/00003086-200302000-00035>
- Meindl, R. S., & Lovejoy, C. O. (1985). Ectocranial suture closure: A revised method for the determination of skeletal age at death based on the lateral-anterior sutures. *American Journal of Physical Anthropology*, *68*(1), 57–66.
<https://doi.org/10.1002/ajpa.1330680106>
- Miroue, M. A. (1975). The human facial sutures: A morphologic and histologic study of age changes from 20 to 95 years. Master of Science (Dentistry) Thesis, University of Washington.

- Mischinski, S., & Ural, A. (2013). Interaction of microstructure and microcrack growth in cortical bone: A finite element study. *Computer Methods in Biomechanics and Biomedical Engineering*, *16*(1), 81–94.
<https://doi.org/10.1080/10255842.2011.607444>
- Moraitis, K., Eliopoulos, C., & Spiliopoulou, C. (2008). Fracture characteristics of perimortem trauma in skeletal material. *The Internet Journal of Biological Anthropology*, *3*(2), 1–8.
- Moss, M. L. (1960). Inhibition and stimulation of sutural fusion in the rat calvaria. *The Anatomical Record*, *136*(4), 457–467. <https://doi.org/10.1002/ar.1091360405>
- Myers, J. C., Okoye, M. I., Kiple, D., Kimmerle, E. H., & Reinhard, K. J. (1999). Three-dimensional (3-D) imaging in post-mortem examinations: Elucidation and identification of cranial and facial fractures in victims of homicide utilizing 3-D computerized imaging reconstruction techniques. *International Journal of Legal Medicine*, *113*(1), 33–37. <https://doi.org/10.1007/s004140050275>
- Ogle, R. C., Tholpady, S. S., McGlynn, K. A., & Ogle, R. A. (2004). Regulation of cranial suture morphogenesis. *Cells Tissues Organs*, *176*(1–3), 54–66.
<https://doi.org/10.1159/000075027>
- Oudhof, H. A. (1982). Sutural growth. *Acta Anatomica*, *112*(1), 58–68.
<https://doi.org/10.1159/000145497>
- Pechnikova, M., Gibelli, D., De Angelis, D., Santis, F., & Cattaneo, C. (2011). The “blind age assessment”: Applicability of Greulich and Pyle, Demirjian and Mincer aging methods to a population of unknown ethnic origin. *La Radiologia Medica*, *116*, 1105–1114. <https://doi.org/10.1007/s11547-011-0694-5>

- Peterson, J., & Dechow, P. C. (2002). Material properties of the inner and outer cortical tables of the human parietal bone. *The Anatomical Record*, 268(1), 7–15.
<https://doi.org/10.1002/ar.10131>
- Pokines, J., & Symes, S. (2013). *Manual of Forensic Taphonomy*. CRC Press, Taylor Francis Group.
- Pritchard, J. J., Scott, J. H., & Girgis, F. G. (1956). The structure and development of cranial and facial sutures. *Journal of Anatomy*, 90(1), 73–86.
- Proff, P., Weingärtner, J., Bayerlein, T., Reicheneder, C., Fanghänel, J., & Bill, J. (2006). Histological and histomorphometric study of growth-related changes of cranial sutures in the animal model. *Journal of Cranio-Maxillofacial Surgery*, 34, 96–100. [https://doi.org/10.1016/S1010-5182\(06\)60021-8](https://doi.org/10.1016/S1010-5182(06)60021-8)
- Quatrehomme, G., & Yaşar İşcan, M. (1997). Beveling in exit gunshot wounds in bones. *Forensic Science International*, 89(1–2), 93–101. [https://doi.org/10.1016/S0379-0738\(97\)00121-7](https://doi.org/10.1016/S0379-0738(97)00121-7)
- Robling, A.G., & Turner, C. (2009). Mechanical signaling for bone modeling and remodeling. *Critical Reviews in Eukaryotic Gene Expression*. 19(4), 319-38.
10.1615/CRITREVEUKARGENEEXPR.V19.I4.50
- Rogers, K. (2010). *Bone and muscle: Structure, force, and motion*. Britannica Educational Publishing.
- Rogers, T. L., & Allard, T. T. (2004). Expert testimony and positive identification of human remains through cranial suture patterns. *Journal of Forensic Sciences*, 49(2), 203–207.

- Ruimerman, R., Van Rietbergen, B., Hilbers, P., & Huiskes, R. (2005). The effects of trabecular-bone loading variables on the surface signaling potential for bone remodeling and adaptation. *Annals of Biomedical Engineering*, 33(1), 71–78. <https://doi.org/10.1007/s10439-005-8964-9>
- Saladin, K. S. (2018). *Anatomy and Physiology. The Unity of Form and Function*. New York: The McGraw-Hill Companies.
- Serageldin, I. (2013). Ancient Alexandria and the dawn of medical science. *Global Cardiology Science and Practice*, (4), 47. <https://doi.org/10.5339/gcsp.2013.47>
- Sherick, D. G., Buchman, S. R., Goulet, R. W., & Goldstein, S. A. (2000). A new technique for the quantitative analysis of cranial suture biology. *Cleft Palate - Craniofacial Journal*, 37(1), 5–11. https://doi.org/10.1597/1545-1569_2000_037_0005_antftq_2.3.co_2
- Slater, B. J., Lenton, K. A., Kwan, M. D., Gupta, D. M., Wan, D. C., & Longaker, M. T. (2008). Cranial sutures: A brief review. *Plastic and Reconstructive Surgery*, 121(4), 170e–178e. <https://doi.org/10.1097/01.prs.0000304441.99483.97>
- Smith, O.C., Berryman, H., & Lahren, C.H. (1987). Cranial fracture patterns and estimate of direction from low velocity gunshot wounds. *Journal of Forensic Science*, 32,1416-1421.
- Sorg, M. H., Haglund, W. D., & Marden, K. (2017). *Forensic taphonomy: the postmortem fate of human remains*. Boca Raton: CRC Press.
- Stefanopoulos, P., Soupiou, O., Pazarakiotis, V., & Filippakis, K. (2015). Wound ballistics of firearm-related injuries—Part 2: Mechanisms of skeletal injury and

characteristics of maxillofacial ballistic trauma. *International Journal of Oral and Maxillofacial Surgery*, 44(1), 67–78. [10.1016/j.ijom.2014.07.012](https://doi.org/10.1016/j.ijom.2014.07.012)

Symes, S. A., L'Abbé, E. N., Chapman, E. N., Wolff, I., & Dirkmaat, D. C. (2012).

Interpreting traumatic injury to bone in medicolegal investigations. In *A Companion to Forensic Anthropology*, 340–389. John Wiley & Sons, Ltd.
<https://doi.org/10.1002/9781118255377.ch17>

Taylor, S. C., & Kranioti, E. F. (2018). Cranial trauma in handgun executions:

Experimental data using polyurethane proxies. *Forensic Science International*, 282, 157–167. <https://doi.org/10.1016/j.forsciint.2017.11.032>

Todd, T. W., & Lyon Jr., D. W. (1924). Endocranial suture closure. Its progress and age

relationship. Part I.—Adult males of white stock. *American Journal of Physical Anthropology*, 7(3), 325–384. <https://doi.org/10.1002/ajpa.1330070320>

Todd, T. W., & Lyon Jr., D. W. (1925). Cranial suture closure. Its progress and age

relationship. Part II. —Ectocranial closure in adult males of white stock. *American Journal of Physical Anthropology*, 8(1), 23–45.

<https://doi.org/10.1002/ajpa.1330080103>

Todd, T. W., & Lyon Jr., D. W. (1925). Cranial suture closure. Its progress and age

relationship. Part III. —Endocranial closure in adult males of Negro stock. *American Journal of Physical Anthropology*, 8(1), 47–71.

<https://doi.org/10.1002/ajpa.1330080104>

Todd, T. W., & Lyon Jr., D. W. (1925). Suture closure—Its progress and age

relationship. Part IV. —Ectocranial closure in adult males of Negro stock.

American Journal of Physical Anthropology, 8(2), 149–168.

<https://doi.org/10.1002/ajpa.1330080203>

Turner, C. H. (2006). Bone strength: Current concepts. *Annals of the New York Academy of Sciences*, 1068(1), 429–446. <https://doi.org/10.1196/annals.1346.039>

Villa, P., & Mahieu, E. (1991). Breakage patterns of human long bones. *Journal of Human Evolution*, 21(1), 27–48. [https://doi.org/10.1016/0047-2484\(91\)90034-S](https://doi.org/10.1016/0047-2484(91)90034-S)

Wagemans, P. A. H. M., van de Velde, J.-P., & Kuljpers-Jagtman, A. M. (1988). Sutures and forces: A review. *American Journal of Orthodontics and Dentofacial Orthopedics*, 94(2), 129–141. [https://doi.org/10.1016/0889-5406\(88\)90361-7](https://doi.org/10.1016/0889-5406(88)90361-7)

Wedel, V. L., & Galloway, A. (2014). *Broken bones: Anthropological analysis of blunt force trauma*. Springfield, IL: Charles C. Thomas, Publisher, LTD.

Wheatley, B. P. (2008). Perimortem or postmortem bone fractures? An experimental study of fracture patterns in deer femora. *Journal of Forensic Sciences*, 53(1), 69–72. <https://doi.org/10.1111/j.1556-4029.2008.00593.x>

White, T. D., Black, M. T., & Folkens, P. A. (2012). *Human osteology*. <http://site.ebrary.com/id/10446604>

VITA

Stephanie Anne Baker**Department of Biological Sciences**

Sam Houston State University

Huntsville, Texas

77341-2116

Education

- Spring 2021: **Ph.D. Prerequisite / Leveling Course in Anthropology**, *in progress*, Texas State University, San Marcos, Texas. Biological Anthropology Seminar (ANTH 5312).
- Fall 2021: **Ph.D. Prerequisite / Leveling Courses in Anthropology**, Texas State University, San Marcos, Texas. Cultural (ANTH 5311) and Archaeology (ANTH 5313) Seminars.
- 2019-Current: **M.Sc. in Biological Sciences**, *in progress*, Sam Houston State University, Huntsville, Texas. Thesis title: *The Quantitative Analysis of Coronal Suture Separation Due to Cranial Trauma*. Thesis advisor: Patrick J. Lewis. Thesis committee: Monte L. Thies, Aaron M. Lynne.
- 2019: **B.S. in Biology** with a minor in Forensic Anthropology and Kinesiology, Sam Houston State University, Huntsville, Texas. Elliott. T. Bowers Honors College Highest Honors and Academic Distinction in Biology. Thesis title: *The Microanatomy of Bone Trauma*. Thesis advisor: Patrick J. Lewis.

Teaching Experience

- 2019 – 2020: Sam Houston State University
TA Teaching Positions
- BIOL 3410 Human Biology Lab (Fall 2019 – present)
 Designed and delivered laboratory lectures over human anatomy; created anatomy lab PowerPoints, exams, assignments, graded all assignments and collaborated closely with professor to prepare students for course.
 - BIOL 2401 Human Anatomy Lab (Spring 2021 – present)
 Delivered laboratory lectures over human anatomy; created lecture presentations, lead dissections on fetal pigs, cats, and sheep hearts, graded all assignments and collaborated closely with professor.
- 2019: Applied Anatomical Research Center (AARC)
Instructor
- Criminal Justice Camp (June-July 2019)

Instructed high school students how a forensic biological profile (age, sex, ancestry, stature) is determined with human skeletal remains.

Grants and Additional Funding

External Grants and Travel Awards

- April 2020: American Association for Anatomy Travel Award: *The Morphology of Ballistic Trauma* - **\$250**
- March 2018: Sigma Xi, Grants-in-Aid of Research: *The Microanatomy of Bone Trauma* - **\$800**

Internal Grants, Scholarships, and Travel Awards

- March 2022: The Graduate College Scholarship, Texas State University - **\$1,000**
March 2022: Texas State Doctoral Merit Fellowship, Texas State University – **\$9,000**
- February 2022: Graduate School Travel Award for Professional Presentation, Sam Houston State University - **\$375**
- January 2022: Graduate School General Scholarship, Sam Houston State University – **\$1,000**
- December 2021: College of Science and Engineering Technology (COSET), Graduate Achievement Scholarship, Sam Houston State University – **\$1,500**
- August 2021: Graduate School General Scholarship, Sam Houston State University – **\$1,000**
- February 2021: Faculty and Student Team Research Award (FAST), PI: Dr. Patrick Lewis, Grant Writer and Project Supervisor: Stephanie Baker, Sam Houston State University - **\$8,000**
- November 2020: Graduate School General Scholarship, Sam Houston State University – **\$1,000**
- November 2020: College of Science and Engineering Technology (COSET), Graduate Achievement Scholarship, Sam Houston State University – **\$1,000**
- September 2020: Graduate School Travel Award for Professional Presentation, Sam Houston State University - **\$50**
- August 2020: Sam Houston State University Department of Biological Sciences Teaching Assistantship Award - **\$7,150**
- May 2020: Joey Harrison Biological Sciences Student Research Award, Sam Houston State University - **\$800**
- January 2020: Sam Houston State University Department of Biological Sciences Teaching Assistantship Award - **\$7,150**
- October 2019: Graduate School Travel Award for Professional Presentation, Sam Houston State University - **\$240**

- January 2019: Elliott T. Bowers Honors Program, Sam Houston State University - **\$500**
- August 2018: Emerging Scholars Honors Program, Elliott T. Bowers Honors College, Sam Houston State University - **\$800**
- April 2018: Elliott T. Bowers Undergraduate Research Symposium Scholarship for Best Overall Poster Award, Sam Houston State University - **\$500**
- October 2017: Elliott T. Bowers Honors Program Honors Distance Learning Scholarship, Sam Houston State University - **\$200**
- August 2017: Emerging Scholars Honors Program, Elliott T. Bowers Honors College, Sam Houston State University - **\$600**
- April 2017: College of Science Engineering and Technology (COSET) Undergraduate Travel Award, Sam Houston State University - **\$205**
- October 2016: Student Travel Award for Professional Presentation (STAPP) Travel Award, Sam Houston State University - **\$205**
- August 2016: Elliott T. Bowers Honors College Scholarship, Sam Houston State University - **\$400**

Publications & Published Abstracts

- Baker, S.A.**, Kiely, J.R. (2020). The Morphology of Ballistic Trauma (Abstract). *American Journal of Physical Anthropology*, 171(S69):15.
- Baker, S.A.**, Kiely, J.R. (2020). The Morphology of Ballistic Trauma (Abstract). *Federation of American Societies for Experimental Biology*, 33(13).
- Baker, S.A.**, Mesa, S.A., Ruble, M.N. (2017). Using Bacterial Communities from Human Femora to Determine Postmortem Interval (Abstract). *American Journal of Physical Anthropology*, 163(S64):108.
- Fakhri, C.T., Rudie, L.M. **Baker, S.A.**, Mann, M., Bivens, S., Spoonire, L., Ruble, M.N. (2017). A Methodology for Extracting Bone Marrow from Cadavers. *Aisthesis Interdisciplinary Honors Journal*, 8(1):42-47.

Manuscripts in Preparation

- Baker, S.A.**, Boyd, A., Anderson, S., Kelly, A., Garcia, G., Campbell, T.L. (submitted). Analysis of the Presence of Supratrochlear Foramen in Modern Forensic and Archeological Sample. To be submitted to *Forensic Science International: Reports*.
- Campbell, T.L., **Baker, S.A.** (in prep). Notes on a Green Heron (*Butorides virescens*) Breeding Colony Along the Brazos River, Baylor University. To be submitted to the *Bulletin of the Texas Ornithological Society*.
- Baker, S.A.**, Campbell, T.L., Lewis, P.J. (in prep). A Comb Based Approach for Standardizing Sampling Locations of Sutural Orthoslices in mCT.
-

Meetings Attended

- February 2022: Texas Academy of Science – 124th annual meeting, Houston, Texas.
- May 2021: Tomography for Scientific Advancement (ToScA) – 11th annual meeting, online, Austin, Texas.
- February 2021: Texas Academy of Science – 124th annual meeting, virtual conference.
- November 2020: Machine Learning Conference EU (ML) – remote edition meeting, online.
- February 2020: Texas Academy of Science – 123rd annual meeting, Nacogdoches, Texas.
- November 2019: Texas Association of Biological Anthropologists – 13th annual meeting, Waco, Texas.
- April 2019: Lambda Alpha Symposium – 21st annual meeting, Wichita, Kansas.
- November 2017: Texas Association of Biological Anthropologists – 11th annual meeting, San Antonio, Texas.
- April 2017: American Association of Physical Anthropologists – 86th annual meeting, New Orleans, Louisiana.
- November 2019: Texas Association of Biological Anthropologists – 10th annual meeting, Austin, Texas.

Academic Conference Presentations

- Baker, S.A.**, Campbell, T.L., Daza, J.D., Lewis, P.J. Quantitative Analysis of Coronal Suture Separation Due to Cranial Trauma. Texas Academy of Science annual meeting, University of Houston Clear Lake, Houston, Texas. February 25-27th, 2022. (Poster)
- Mongan, K.A., **Baker, S.A.**, Campbell, T.L. Supracondylar Process Percent Incidence in a Modern Forensic Collection. Texas Academy of Science annual meeting, University of Houston Clear Lake, Houston, Texas. February 25-27th, 2022. (Poster)
- Baker, S.A.**, Campbell, T.L., Daza, J.D., Lewis, P.J. A mCT Comb Based Approach to Standardize Sampling locations of the Coronal Suture.
- Tomography for Scientific Advancement – North America. May 24-25, 2021. (Poster – virtual)
 - Southwestern Association of Naturalists. April 22-24, 2021. (Poster - virtual)
 - Texas Academy of Sciences conference. February 26-27, 2021. (Poster - virtual)
- Campbell, T.L., **Baker, S.A.**, Cunningham, D.L., Daza, J.D. Comparison of two packing methodologies for microfaunal mCT scanning. Tomography for Scientific Advancement – North America. May 2021. (Poster – virtual)
- Sarles, M., **Baker, S.A.**, Lewis, P.J. Flexion of the Coronal Suture in Response to Traumatic Forces. Sam Houston State University Undergraduate Research Symposium, Huntsville, Texas. Online. April 2021.

- Pellikan, K., Pflieger, A., Jones, C., Skoglund, S., Roinson, R., **Baker, S.A.**, Campbell, T. L. Sexual Dimorphism of Human Humeri. Baylor University's Undergraduate Research and Scholarly Achievement (URSA) annual meeting, Online. April 5th-19th, 2021. (Poster)
- Dang, S., Mazza, E., Ramesh, D., Lemus, W., Szymanek, S., **Baker, S.A.**, Campbell, T.L. Human Humeri Bilateral Asymmetry. Baylor University's Undergraduate Research and Scholarly Achievement (URSA) annual meeting, Online. April 5th-19th, 2021. (Poster)
- Boyd, A., Anderson, S., **Baker, S.A.**, Kelly, A., Garcia, G., Campbell, T.L. Analysis of Sex-Based Differences in the Percent Incidence of Humeral Supratrochlear Foramina. Texas Academy of Science annual meeting, Online. February 26-27, 202. (Presentation)
- Baker, S.A.**, Lewis, P.J. The Quantitative Analysis of Coronal Suture Separation due to Cranial Trauma. Society of Integrative and Comparative Biology annual meeting, Online. January – February 2021. (Poster)
- Baker, S.A.**, Kiely, J.R. The Morphology of Ballistic Trauma. American Association of Physical Anthropology.
- American Association of Physical Anthropology. April 2020. (Poster)
 - American Association of Anatomists. April 2020 (Poster)
 - Texas Association of Biological Anthropologists. November 2019 (Oral)
 - Sam Houston State University's Undergraduate Research Symposium. April 2019 (Oral)
- Baker, S.A.** The Morphology of Ballistic Trauma on Craniums. American Association of Anatomists annual meeting, San Diego, California. April 2020. (Poster)
- Baker, S.A.**, Lewis, P.J. The Quantitative Analysis of Cranial Trauma. Texas Academy of Science 123rd annual meeting, Nacogdoches, Texas. February 2020. (Poster)
- Hooper, M., **Baker, S.A.** Examining the Effects of Blunt Force Trauma of the Mandible using mCT. Sam Houston State University Undergraduate Research Symposium, Huntsville, Texas. April 2020. (Poster)
- Osborne, V., **Baker, S.A.** Examining Asymmetries in Human Cortical Bone. Sam Houston State University Undergraduate Research Symposium, Huntsville, Texas. April 2020. (Poster)
- Sanders, K., **Baker, S.A.** The Effects of Tibial Fractures on Knee Replacements. Sam Houston State University Undergraduate Research Symposium, Huntsville, Texas. April 2020. (Poster)
- Sanders, K., **Baker, S.A.** The Microanatomy of Tibial Trauma Using mCT. Sam Houston State University Undergraduate Research Symposium, Huntsville, Texas. April 2020. (Poster)
- Baker, S.A.**, Lewis, P.J. The Microanatomy of Bone Trauma.
- Wichita State Lambda Alpha Symposium. April 2019. (Oral)
 - Texas Undergraduate Research Day at the Texas Capitol. April 2019. (Poster)

- Sam Houston State University's Undergraduate Research Symposium. April 2018. **(Best Poster Award)**
- Texas Academy of Biological Anthropologists. November 2017. (Poster)

Boutch, O., Munoz, J., **Baker, S.A.** The Microanatomy of Ballistic Trauma to the Sternum. Sam Houston State University Undergraduate Research Symposium, Huntsville, Texas. April 2018. (Poster)

Smith, C., **Baker, S.A.** Examination of Sharp Force Trauma to the Skull Using mCT. Sam Houston State University Undergraduate Research Symposium, Huntsville, Texas. April 2018. (Poster)

Baker, S.A., Ruble, M.N., Lewis, P.J. Using Bacterial Communities from Human Femora to Determine Postmortem Interval.

- American Association of Physical Anthropologists. April 2017. (Poster)
- Texas Academy of Biological Anthropologists. November 2016. (Poster)

Invited Lectures and Presentations

March 2022: *The Quantitative Analysis of Coronal Suture Separation Due to Cranial Trauma.* Department of Anthropology – ANT 4355, Forensic Anthropology, Baylor University, Waco, Texas.

November 2021: *Masters Research using mCT Technology and Graduate Student Life.* Department of Anthropology – ANT 4355, Forensic Anthropology, Baylor University, Waco, Texas.

October 2020: Tri Beta undergraduate presentation: *How to construct a CV and read a scientific paper.* Department of Biological Sciences, Sam Houston State University, Huntsville, Texas.

February 2020: *The Morphology and Microanatomy of Ballistic Trauma.* Department of Anthropology – ANT-4358, Death, Injury, & Physical Remains, Baylor University, Waco, Texas.

Workshops and Professional Development

August 2021: **Texas State University Summer Human Osteology Workshop.** San Marcos, Texas, August 16-20. Course Instructor: Dr. Daniel Wescott (Texas State University). Overview of the human skeleton, basic bone biology, anatomical terminology, anatomy of the skull, postcranial anatomy, and common anatomical variations of the human skeleton.

May 2021: **3D Slicer and SlicerMorph Workshop.** Austin, Texas, May 26-27. Course Instructor: Murat Maga and Sara Rolfe. Basic digital morphology and geometric morphometric data collection.

October 2020: **Cameron Park Zoo's Great Ape Cardiac Health Workshop.** Waco, Texas, October 20th. Course Instructor: Emily Ellison (Primate Keeper) Demonstrations geared towards improving cardio health in

great apes with a focus on voluntary non-anesthetized blood draws, arm and finger blood pressure methods, EKG and details of echocardiograms.

- September 2020: **Transmitting Science Introduction to Machine Learning Applied to Paleontology and Archeology.** Hostalets de Pierola, Barcelona, Spain, September 7 – 11. Course Director: Dr. Soledad De Esteban-Trivingo (Transmitting Science, Spain). Instructor: Dr. Manuel Domingues-Rodrigo (Complutense University, Spain). Introduction to Machine Learning in order to obtain and analyze data with data and process mining.
- August 2020: **University of Texas High-Resolution X-ray CT Facility Virtual Biology/Paleo Short Course.** Austin, Texas. 10-14 August 2020. Course Director: Dr. Jessica Maisano. Instructors: Dr. Matthew Colbert (University of Texas) and David Edey (University of Texas). Introduction to the fundamentals of data acquisition, visualization, and analysis of high-resolution X-ray CT (HRXCT) data for biological and paleontological samples using Avizo, Dragonfly, and ImageJ.

Field Work and Experience & Collections Research

- March 2022: Bonfire Shelter Restoration, Comstock, Texas. Assisted in backfill of the Bonfire Archaeological site. PI's: Dr. David Kilby and Dr. Steve Black.
- October – November 2021: Forensic Anthropology Center at Texas State (FACTS), San Marcos, Texas. Examination and photography of skeletal collection for the presence of supratrochlear foramen
- November 2020: Southeast Texas Applied Forensic Science Facility (STAFS), Huntsville Texas. Examination and photography of skeletal collection for the presence of supratrochlear foramen.
- August 2019: Course: Forensic anthropology and burial recovery for law enforcement. Assisted in recovery of human skeletal remains of a clandestine burial using archaeological techniques. Southeast Texas Applied Forensic Science Facility (STAFS): Huntsville, Texas. Director and course instructor: Dr. Joan A. Bytheway.
- July 2019: Course: Blood stain analysis and pattern evidence summer course. Recognition, processing, and analysis of bloodstains at crime scenes and latent print identification and processing. Southeast Texas Applied Forensic Science Facility (STAFS): Huntsville, Texas. Director and course instructor: Dr. Joan A. Bytheway.

- July 2019: Course: Bone pathology. Assisted in identifying bone/dental anomalies and pathologies of the human skeleton and investigate disease(s) effects bone/teeth. Southeast Texas Applied Forensic Science Facility (STAFS): Huntsville, Texas. Director and course instructor: Dr. Joan A. Bytheway.
- July 2019: Course: Surface recovery. Assisted in teaching systematic recovery techniques, identification of human bone, distinguishing human bone from animal bone and assessing the age, sex, ancestry, and stature of skeletal remains. Southeast Texas Applied Forensic Science Facility (STAFS): Huntsville, Texas. Director and course instructor: Dr. Joan A. Bytheway.
- June 2019: Course: Human decomposition. Explored techniques of determining the postmortem interval and how decomposition affects soil composition. Southeast Texas Applied Forensic Science Facility (STAFS): Huntsville, Texas. Director and course instructor: Dr. Joan A. Bytheway.
- June 2019: Course: Human burial recovery. Search and recovery of human skeletal remains of a burial and process/analyze remains for identification. Southeast Texas Applied Forensic Science Facility (STAFS): Huntsville, Texas. Director and course instructor: Dr. Joan A. Bytheway.
- June 2019: Course: Forensic anthropology and human burial recovery. Applied basic methods for estimating sex, age, stature, and ancestry, while also using fundamental systematic recovery methods. Southeast Texas Applied Forensic Science Facility (STAFS): Huntsville, Texas. Director and course instructor: Dr. Joan A. Bytheway.
- June – July 2019: Course: Sam Houston State University Criminal Justice camp for high school students. Taught basic forensic anthropology methods for estimating sex, age, stature, and ancestry of human skeletal remains. Applied Anatomical Research Center (AARC): Huntsville, Texas. Director and course instructor: Dr. Joan A. Bytheway.
- February 2018: Applied Anatomical Research Center (AARC): Huntsville, Texas. PI: Dr. Joan A. Bytheway. Team leader for mock crime scene recovery. Organized and instructed proper collection and recovery methods for human skeletal remains.
- February 2017: Whiskey River Bridge: Caldwell, Texas. PI: Dr. Patrick Lewis. Excavation and analysis of an early Pliocene faunal deposit.

- May – October 2016: Southeast Texas Applied Forensic Science Facility (STAFS): Huntsville, Texas. PI: Dr. Patrick Lewis. Maceration of cadaver skeletal appendages.
- May – November 2016: Southeast Texas Applied Forensic Science Facility (STAFS): Huntsville, Texas. PI: Dr. Patrick Lewis. Cadaver bone marrow sampling using medical grade T-lock biopsy tools.
-

Professional Experience

- 2018 – 2019: Student Worker and Researcher – Applied Anatomical Research Center (AARC). Assisted in disarticulation of craniums, measuring skeletal elements of juvenile skeletons, macerating, search and recovery of human remains, and cataloging bones.
- January 2019 – May 2019: Assistant – Sam Houston State University College of Osteopathic Medicine (COM). Assisted in dissecting and prepping cadavers for medical student instructional videos, operating camera equipment, and editing videos.
-

Forensic Case Work Assisted

- January 2019: Search and recovery of human remains, Hillister, Texas.
- January 2019: Superimposition of skull photo over facial photograph, Huntsville, Texas.
- December 2018: Recovery, maceration, and reassembled skull of adult female with blunt force trauma, Huntsville, Texas.
- December 2018: Maceration and reconstruction of juvenile (2-year-old) skull, Huntsville, Texas.
-

Lab Experience

- July 2016-present: Dr. Patrick J. Lewis' Paleobiology Laboratory, Sam Houston State University. *Graduate Lab Coordinator* – Organizing lab meetings and events, Amira/Avizo CT software training and undergraduate lab training.
- Undergraduate Research Project Leader* – Organizing lab meetings and events, undergraduate CT software training and lab training. January 2018 – May 2019.
- April – June 2016: Dr. Joni Seeling's Human Anatomy Laboratory, Sam Houston State University. Undergraduate Research – Examined the effect of artificial sweetener on *Xenopus laevis* embryos.

Honors & Awards

- May 2021: Department of Biological Sciences Outstanding Graduate Student Award.

- May 2021: College of Science and Engineering Technology Graduate Student Excellence in Research Award.
- May 2020: Joey Harrison Biological Sciences Student Research Award, Sam Houston State University.
- April 2020: American Association for Anatomy Student Travel Award.
- October 2019: Graduate School Travel Award for Professional Presentation, Sam Houston State University.
- August 2019: Elliott T. Bowers Honors College Highest Honors and Academic Distinction in Biology.
- May 2019: President's List – Sam Houston State University.
- December 2018: President's List – Sam Houston State University.
- April 2018: Best overall Poster Presentation Award, Sam Houston State University Undergraduate Research Symposium.
- March 2018: Sam Houston State University Raven Scholar Nominee.
- April 2017: College of Science Engineering and Technology (COSET) Undergraduate Travel Award, Sam Houston State University.
- 2016-2019: Member of the Elliott T. Bowers Honors College at Sam Houston State University.
- October 2016: Student Travel Award for Professional Presentation (STAPP) Travel Award, Sam Houston State University.
- May 2016: President's List – Sam Houston State University.
- 2015-2019: Dean's List – College of Science Engineering and Technology, Sam Houston State University.

Mentored Students, Honors & Awards

- February 2022: Kailey Mongan – Undergraduate at Baylor University – Project: *Supracondylar Process Percent Incidence in a Modern Forensic Collection*. 2nd Place Best Anthropology Poster – Texas Academy of Science annual meeting, University of Houston Clear Lake, Houston, Texas.
- Jan 2022 – present: Faith Calma – Undergraduate at Sam Houston State University – Project: *Examining a Gunshot Wound effects on the Sagittal Suture*.
- Jan 2022 – present: Kaitlyn Hallford – Undergraduate at Sam Houston State University – Project: *Examining a Gunshot Wound effects on the Sagittal Suture*.

- Jan 2022 – present:* Kaitlyn Knight – Undergraduate at Sam Houston State University – Project: *Examining Blunt Force Trauma effects on the Sagittal Suture.*
- Aug – December 2021:* Ismael De Leon – Undergraduate at Sam Houston State University – Graduate student supervisor for the Faculty and Student Team Research Award (FAST).
- May – August 2021:* Jakob Unruh – Undergraduate at Sam Houston State University – Graduate student supervisor for the Faculty and Student Team Research Award (FAST).
- May – August 2021:* April Tang – Undergraduate at Sam Houston State University – Graduate student supervisor for the Faculty and Student Team Research Award (FAST).
- January – May 2021:* Molly Sarles – Undergraduate at Sam Houston State University – Project: *Examining Asymmetries in the Coronal Suture of Crania with Traumatic Injuries.*
- August – December 2020:* Margaret Leming – Undergraduate at Sam Houston State University – Project: Human Biology Laboratory Manual.
- August 2019 – May 2020:* Katelyn Sanders – Undergraduate at Sam Houston State University – Project: *The Effects of Tibial Fractures on Knee Replacements.*
- August 2019 – May 2020:* Katelyn Sanders – Undergraduate at Sam Houston State University – Project: *The Microanatomy of Tibial Trauma.*
- August – December 2019:* Marissa Hooper – Undergraduate at Sam Houston State University – Project: *Examining the Effects of Blunt Force Trauma of the Mandible using mCT.*
- August – December 2019:* Victoria Osborne – Undergraduate at Sam Houston State University – Project: *Examining Asymmetries in Human Cortical Bone.* Best Senior Poster – Undergraduate Research Symposium (URS), Sam Houston State University.
- August – December 2019:* Jesse Rodriguez – Undergraduate at Sam Houston State University – Project: *Examining Microfractures in Cortical Bone from Ballistic Trauma using mCT.*
- August – December 2019:* Briston Thornton – Undergraduate at Sam Houston State University – Project: *Examining Microfractures in Cortical Bone from Ballistic Trauma using mCT.*
- January – May 2019:* Christine Smith – Undergraduate at Sam Houston State University – Project: *Examination of Sharp Force Trauma to the Skull.*
- January – May 2019:* Jessica Munoz – Undergraduate at Sam Houston State University – Project: *The Microanatomy of Ballistic Trauma to the Sternum.*

January – May 2019: Olivia Boutch – Undergraduate at Sam Houston State University – Project: *The Microanatomy of Ballistic Trauma to the Sternum.*

Service

University/Professional Service & Public Outreach

February 2022 - present: Anthropology Section Chair for Texas Academy of Science.

February 2022: Oral and Poster Presentation Judge – Texas Academy of Science. Undergraduate Level in the Anthropology section.

April 2021: Moderator – Undergraduate Research Symposium, Sam Houston State University.

February 2021: Oral Presentation Judge – Texas Academy of Science. Undergraduate Level in the Anthropology section.

2020 – May 2021: President, Biological Sciences Graduated Student Organization, Sam Houston State University.

2019 – May 2021: Graduate student representative for the Biological Sciences Graduate Committee, Sam Houston State University.

2019 – May 2021: Vice President, Beta Beta Beta National Biological Honors Society Delta Tau Chapter at Sam Houston State University.

January 2018 – present: Tri Beta Biological Honors Society – Tutored Sam Houston State University Biology undergraduates.

2018 – present: Habitat Restoration at Sam Houston State University Biological Field Station – Maintained habitat for the endangered Red-Cockaded Woodpecker.

2019 – December 2019: Secretary, Biological Sciences Graduated Student Organization, Sam Houston State University.

June – July 2019: Sam Houston State University Criminal Justice Camp – Instructed high school students the basic methods for estimating sex, age, stature, and ancestry of skeletonized human remains.

February 2019: Poster and Oral Presentation Judge – Texas Academy of Science. Undergraduate & Graduate Level in the Anthropology section.

January – May 2019: Huntsville Home School Co-op – Comparative Vertebrate Anatomy Class Instructor. Created, organized, and instructed high school students about anatomical homologous structures across vertebrate taxa. Used anatomical structures and various laboratory dissections to facilitate understanding.

January – May 2017: Huntsville Home School Co-op – Comparative Vertebrate Anatomy Class Instructor. Created, organized, and instructed high school students about anatomical homologous structures

across vertebrate taxa. Used anatomical structures and various laboratory dissections to facilitate understanding.

April 2017: Gardening at Gibbs Middle School – Maintained garden and planted new trees.

Research Interests

- Human Skeletal Trauma
- Fracture Morphology
- Functional Morphology
- Human Osteology
- Taphonomy
- Biomechanics
- Osteometry
- Morphometrics
- Machine Learning
- Deep Learning
- mCT

Technical Skills

- Avizo Segmenting Software
- Dragonfly Segmenting Software
- 3DSlicer
- ImageJ/Fiji
- TPSDig
- Fordisc 4.0
- ISOMET 5000 Microtome Saw
- Adobe Illustrator
- R and LaTeX R
- Python
- Microsoft Word, Excel, PowerPoint

Certifications

- Bloodborne and Airborne Pathogens Certification
- CITI IACUC Animal Research
- CITI Working with Amphibians in Research Settings

Professional Affiliations and Memberships

- Tomography for Scientific Advancement
- Alpha Chi National College Honor Society
- Southwestern Association of Naturalists
- Texas Academy of Science
- American Association of Anatomists
- SHSU Biological Sciences Graduate Student Organization
- President, May 2020 – May 2021
 - Secretary, January 2020 – May 2020
- American Association of Physical Anthropologists
- Sigma Xi, Associate Member
- Society of Integrative and Comparative Biology
- SHSU Beta Beta Beta National Biological Honor Society
- Vice President, August 2019 – May 2021
- Sam Houston Association for Medically Oriented Students
- Society of Forensic Science at Sam Houston State University
- Kinesiology, Health, Recreation Association for Sam Houston State University